Ore Geology Reviews 63 (2014) 374–387

Contents lists available at ScienceDirect

Ore Geology Reviews

journal homepage: www.elsevier.com/locate/oregeorev

Reprint of "The Gongchangling BIFs from the Anshan–Benxi area, NE China: Petrological–geochemical characteristics and genesis of high-grade iron ores"

Xiao-Hui Sun [a,b], Xiao-Qing Zhu [a,*], Hao-Shu Tang [a], Qian Zhang [a], Tai-Yi Luo [a]

[a] State Key Laboratory of Ore Deposit Geochemistry, Institute of Geochemistry, Chinese Academy of Sciences, Guiyang 550002, China
[b] University of Chinese Academy of Sciences, Beijing 100049, China

ARTICLE INFO

Article history:
Received 15 June 2013
Received in revised form 7 December 2013
Accepted 31 December 2013
Available online 9 June 2014

Keywords:
Neoarchean BIFs
High-grade iron ore
Oxide facies
Gongchangling
North China Craton

ABSTRACT

The Gongchangling BIFs are located in the Anshan–Benxi area, northeastern part of the North China Craton, of which the No. 2 mining area is the largest and most typical high-grade iron ore producing area in China. In this study, the mineralogy, petrology and chemistry of iron ores (BIFs and high-grade iron ores) and their wall-rocks (amphibolite and garnet–chlorite schist) from the Gongchangling No. 2 mining area were examined to constrain the genesis of high-grade iron ore.

The BIFs are composed essentially of magnetite and quartz, in addition to actinolite in a few samples; while the high-grade iron ores are mainly composed of magnetite and the quartz is relatively rare. The low contents of Al_2O_3, TiO_2 and HFSE in the BIFs and high-grade iron ores indicate that they are marine chemical precipitates with little input of terrigenous clastic sediments. The magnetite and quartz from BIFs and high-grade iron ores exhibit the similar chemical composition. The REY patterns of BIFs and high-grade iron ores suggest their precipitation after mixing of hydrothermal component with seawater in certain proportions under relatively low oxygen level, and the obvious positive Eu anomalies indicate that high-temperature hydrothermal fluids which percolate and dissolve the submarine volcanic rock may supply the ore-forming material to the Gongchangling iron deposit.

The amphibolite as interlayer of BIFs recorded the metamorphic temperature of 567 ± 25 °C, moreover, the garnet from wall-rock of high-grade iron ore exhibits the growth zoning produced during prograde metamorphism, indicating that metamorphic hydrothermal fluids played an important role in the genesis of high-grade iron ore. It was proposed that the Gongchangling iron deposit was formed in an arc-related tectonic setting at the late Neoarchean, then it underwent lower amphibolite facies metamorphism, and the high-grade iron ore is the reformed product of BIFs by metamorphic hydrothermal fluids.

1. Introduction

Banded iron formations (BIFs) are highly controversial Precambrian chemical sedimentary rocks characterized by the commonly alternating presence of iron-rich layers and silica-rich layers. They are defined as follows: a chemical sediment, typically thin bedded or laminated, containing 15% or more iron of sedimentary origin, commonly but not necessarily containing layers of chert (James, 1954). Banding is best preserved in low-grade metamorphic occurrences, but even high-grade metamorphosed BIFs retain relict banding (Bekker et al., 2010). The various scales of banding may exist, from macro- through meso- to microbands defined by Trendall and Blockley (1970).

The BIFs occurred in the Precambrian geologic record over a wide time span. The age of BIFs ranges from 3.8 Ga to 1.8 Ga, reappearing at the end of the Neoproterozoic era (ca. 0.8–0.6 Ga), and the peak in BIFs abundance is ca. 2.5 Ga (Bekker et al., 2010; Huston and Logan, 2004; Klein, 2005). The cessation of BIFs deposition at 1.8 Ga results from oxygenation of atmosphere and the development of sulfidic deep ocean or the Sudbury Impact Event creating a suboxic redox state for deep seawater, whereas after a hiatus of over a billion years, the reappearance of Iron Formation in the Neoproterozoic has genetic relationship with the Snowball Earth Event (Bekker et al., 2004; Cloud, 1973; Huston and Logan, 2004; Slack and Cannon, 2009; Tang and Chen, 2013; Tang et al., 2008, 2009a,b, 2011, 2013a,b; Young, 2013; Zhao, 2010). James (1954) established four distinctive facies for BIFs on the basis of dominant original iron minerals: oxide facies, silicate facies, carbonate facies and sulfide facies. The BIFs were divided into Algoma type and Lake Superior type based on the characteristics of their depositional environments and the types of associated rocks (Gross, 1980). The Algoma type BIFs are relatively small in size and thickness, and are

DOI of original article: http://dx.doi.org/10.1016/j.oregeorev.2013.12.017.
* Corresponding author at: State Key Laboratory of Ore Deposit Geochemistry, Institute of Geochemistry, Chinese Academy of Sciences, 46th Guanshui Road, Guiyang 550002, China. Tel.: +86 851 5891701; fax: +86 851 5891664.
E-mail address: zhuxqcas@sohu.com (X.-Q. Zhu).

0169-1368/$ – see front matter © 2014 Elsevier B.V. All rights reserved.
http://dx.doi.org/10.1016/j.oregeorev.2014.06.002

associated with volcanic and greywacke rock assemblages along volcanic arcs, rift zones, deep-seated fault and fracture system, whereas the Lake Superior type BIFs were deposited with quartzite, dolomite and black shale in relatively shallow marine environment under more stable tectonic conditions, over passive margin continental-shelf environment (Gonzalez et al., 2009; Gross, 1980). The deposition of BIFs has been linked to significant compositional change in the Earth's atmosphere, hydrosphere and the diversification of biosphere (Bekker et al., 2010; Chen, 1996; Chen et al., 1991, 1994, 1996; Tang and Chen, 2013). Therefore, research on BIFs plays a significant role in understanding the evolution of atmosphere and biosphere, as well as coeval ocean composition (Bekker et al., 2010; Cairnssmith, 1978; Chen and Zhu, 1984; Craddock and Dauphas, 2011; Farquhar and Wing, 2003; Holland, 2002; Huston and Logan, 2004; Lascelles, 2007; Li et al., 2010; Mojzsis et al., 1996; Posth et al., 2008; Tang and Chen, 2013; Tang et al., 2013a,b; Walker, 1984; Young, 2013).

In China, BIFs are mainly distributed in the North China Craton (NCC), including the western Liaoning, the eastern Hebei, the northern Shanxi, the western Anhui, the southwestern Henan and the western Shandong Provinces (Zhang et al., 2012a,b), among which the western Liaoning Province is one of the most important iron ore provinces in China (Xie et al., 2009). The Gongchangling iron deposit located in the Anshan–Benxi area of Liaoning Province, is an oxide facies Algoma type BIFs, and the Gongchangling No. 2 mining area is the largest and most typical high-grade iron ore distribution area in China (Zhou, 1987, 1994, 1997). As for the genesis of high-grade iron ore, however, there are still highly controversial interpretations, including: (1) the high-grade iron ore was mainly formed during original deposition stage (Chen et al., 1984); (2) it was formed during hydrothermal reformation stage (Li et al., 2012; Liu and Jin, 2010; Wang et al., 2012). In this process, the silicon of BIFs was carried away by the hydrothermal fluid, while the iron of BIFs was reserved. However, there are two distinctively different opinions concerning the nature of the hydrothermal fluid, one is migmatitic hydrothermal fluid (Chen et al., 1985; Cheng, 1957; Li et al., 1977; Zhao and Li, 1980; Zhao et al., 1979), and the other is metamorphic hydrothermal fluid (Guan, 1961; Shi and Li, 1980; Zhou, 1994); (3) the graphite-bearing high-grade iron ore was formed from siderite which was decomposed during metamorphism (Li, 1979, 1982; Li et al., 1983).

In this contribution, therefore, we carried out integrated ore deposit geology, mineralogy and geochemical investigations on the BIFs, high-grade iron ore and their hosting rocks from the Gongchangling No. 2 mining area, thereby provide insights into the origins of ore-forming material and genesis of high-grade iron ore.

2. Region and deposit geology

The North China Craton, one of the oldest cratons in the world, is bound to the north by the Central Asian Orogenic Belt (CAOB) and to the south by the Qinling–Dabie–Sulu orogenic belt (Zhao and Zhai, 2013). Traditionally, the NCC was considered to be composed of uniform Archean–Paleoproterozoic basement overlain by Paleo-Mesoproterozoic unmetamorphosed cover (Zhao and Zhai, 2013; Zheng et al., 2013). As to the tectonic division of the NCC basement, it is controversial, and there are two representative views. According to Zhai and co-workers (Zhai, 2011; Zhai and Santosh, 2011; Zhai et al., 2000, 2005), the Archean basement of the NCC was divisible into seven blocks: Jiaoliao (JL), Qianhuai (QH), Ordos (OR), Jinning (JN), Xuchang (XCH), Xuhuai (XH) and Alashan (ALS) blocks, and these micro-blocks were welded by ca. 2.7 Ga and 2.5 Ga late Archean greenstone belts (Fig. 1). Zhai and Santosh (2011) proposed that the Precambrian crustal evolution of the NCC related to three major geological events: (1) a major phase of continental growth at ca. 2.7 Ga; (2) the amalgamation of micro-blocks and cratonization at ca. 2.5 Ga; and (3) Paleoproterozoic rifting–subduction–accretion–collision tectonics and subsequent high-grade granulite facies metamorphism–granitoid magmatism during ca. 2.0–1.82 Ga. However, Zhao et al. (2003, 2005) proposed that the Precambrian basement of the NCC was divided into the Archean to Paleoproterozoic Eastern and Western blocks and three Paleoproterozoic orogenic belts, named the Jiao-Liao-Ji Belt, Khondalite Belt and Trans-North-China Orogen, of which the NS-trending Trans-North-China Orogen divide the basement of the NCC into the Eastern and Western blocks, whereas the Jiao-Liao-Ji Belt and the EW-trending Khondalite Belt are located within the Eastern and Western blocks, respectively. It was proposed that the Jiao-Liao-Ji Belt was a Paleoproterozoic rift-and-collision belt, the Khondalite Belt resulted from amalgamation of the Yinshan and Ordos blocks to form the Western Block at ca. 1.95 Ga, and the Trans-North-China Orogen resulted from the collision of the Eastern and Western blocks above an eastern subduction zone at ca. 1.85 Ga (Zhao and Zhai, 2013).

According to tectonic division of the NCC proposed by Zhai and Santosh (2011), the Anshan–Benxi area is located in the northern part of JL block containing the early Precambrian Anshan Group and Liaohe Group (Fig. 1, Zhai and Windley, 1990). The Anshan Group is divisible into the lower, middle and upper Anshan Group, and the BIFs in this area mainly occur in the middle and upper Anshan Group (Zhou, 1994). The main rock types of the Anshan Group consist of amphibolites, leptynites, schists, migmatites, BIFs and other rock types including siliceous rocks and carbonates on the whole (Zhou, 1994). In this area, an unconformity separates the underlying Archean Anshan Group from the overlying Paleoproterozoic Liaohe Group, and both the Anshan and Liaohe groups are overlain unconformably by undeformed sediments (Tang et al., 2008, 2009a,b, 2011, 2013a,b; Zhai and Windley, 1990; Zhai et al., 1990a).

The Anshan basement is divisible into three parts: the Tiejiashan gneiss, the Anshan gneiss and the Anshan supracrustal rocks (Zhai and Windley, 1990). The Tiejiashan gneiss occurs at the Tiejiashan area, on east of the Anshan City, with an area of over 25 km^2, forming the basement of the Anshan Group. The Anshan gneiss intrudes the Anshan supracrustal rocks and their intercalated BIFs, resulting in the latter being observed as variable-sized enclaves in the former (Zhai and Windley, 1990; Zhai et al., 1990a). As Song et al. (1996) reported the zircon U–Pb age of 2962 ± 4 Ma and 2964 ± 6 Ma for the Tiejiashan gneiss (the basement of the Anshan Group), and yielded zircon U–Pb age of 2474 ± 13 Ma for the Qidashan granitic gneiss which intruded the Anshan Group, it is indicated that the Anshan Group is the Neoarchean or earliest Proterozoic in age on the basis of their tectonic relationship.

The Gongchangling iron deposit from the Anshan–Benxi area can be divided into four mining areas: the Nos. 1–3 mining areas, and the Laoling–Bapanling mining area (Chi, 1993; Zhou, 1994). The No. 2 mining area, the main high-grade iron ore distribution area, is located in the north limb of the Gongchangling anticline (Chi, 1993; Zhou, 1994). It is bounded by the Hanling Fault to the northwest, the Pianling Fault to the southeast, and is adjacent to the Laoling–Bapanling mining area (Fig. 2). The ore bodies in the Gongchangling No. 2 mining area are 4500 m in length and 300–600 m in width, and hosted by the metamorphic rocks of the Cigou Formation of the middle Anshan Group (Wan, 1994). In general, the iron ores are intimately associated with amphibolites and metasediments, and the detailed rock units are as follows from base to top (Fig. 3; Zhou, 1994): (1) Lower amphibolite; (2) Lower schist; (3) Lower iron ore belt: composed of Fe1 (Fe1–Fe6 means the first to the sixth layer of BIFs), middle schist and Fe2; (4) Middle leptynite: interlayer with Fe3; (5) Upper iron ore belt: composed of Fe4, lower amphibolite, Fe5, upper amphibolites and Fe6; (6) Siliceous rock. Recently, Wan et al. (2012b) reported a zircon SHRIMP U–Pb age of 2528 ± 10 Ma of leptynites which were collected from the Gongchangling BIFs' interlayer, indicating that formation age of the BIFs is the late Neoarchean.

The Gongchangling iron deposit occurs as enclaves within large area of migmatite (Zhou, 1994). In Gongchangling No. 2 mining area, the iron ore bodies which are narrowly strip-shaped dip to NE, with a dip angle of 60–85°. These ore bodies extend over underground 1000 m, and the high-grade iron ore mainly occurred as lens or quasi-bedded shape

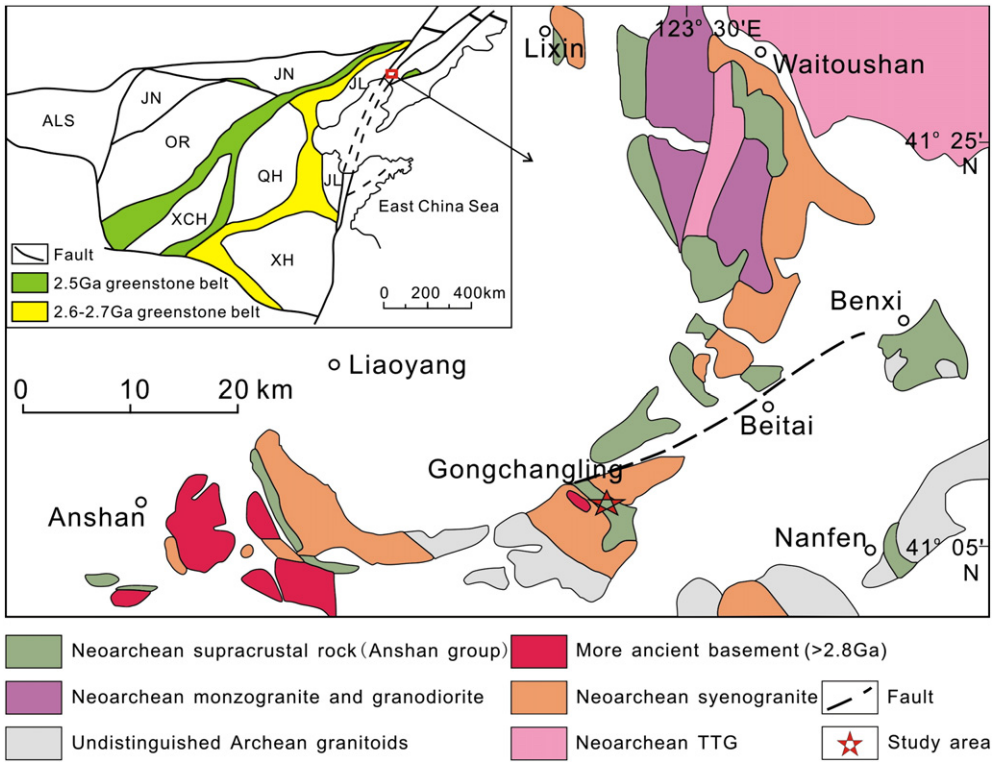

Fig. 1. Geological map of the Anshan–Benxi area, Liaoning Province (modified after Wan, 1994; Zhai and Santosh, 2011). JL, Jiaoliao block; QH, Qianhuai block; OR, Ordos block; JN, Jinning block; XCH, Xuchang block; XH, Xuhuai block; ALS, Alashan block.

within the BIFs layer of Fe6. The mode of occurrence of high-grade iron ores is roughly consistent with that of BIFs, and there is a smooth transition from high-grade iron ores to BIFs (Chi, 1993). Strike reverse faults and transverse faults are well developed in this area, the former developed during regional metamorphism along the ore layer of Fe6, whereas the latter developed after mineralization period, and the occurrence of high-grade iron ores is mainly controlled by the strike reverse faults (Zhou, 1994). The high-grade iron ores are 1–30 m in thickness, dozens of meters to over 1000 m in length. The wall-rocks of high-grade iron ores exhibit obvious alteration zoning in sequence of amphibolization (cummingtonite), garnetization and chloritization outwards from the ore bodies, and the more intense the alteration of wall-rocks, the larger the scale of high-grade iron ores (Zhao and Li, 1980; Zhou, 1994). The iron ores are mainly characterized by banded (BIFs) or massive (high-grade iron ore) structure and granular texture, and the ore types consist of low-grade magnetite ore, high-grade magnetite ore, low-grade martite ore and high-grade martite ore. Furthermore, magnetite ore is the major type (Chi, 1993).

3. Sample collection and analytical methods

The BIFs and high-grade iron ores were all collected from the No. 13 exploration tunnel of the Gongchangling No. 2 mining area, with a depth of 280 m. The BIFs showing macro- or micro-banded structures are usually low-grade iron ores. Whereas, the high-grade iron ores generally display compact massive structure, and occasionally show loose and porous structure and granular texture. In this article, the high-grade iron ore (namely, the high-grade BIFs) is defined by TFe ≥ 45%, while the BIFs means 20% < TFe < 45% (Zhou, 1994). The garnet–chlorite schists were collected from the wall-rock of high-grade iron ore, while

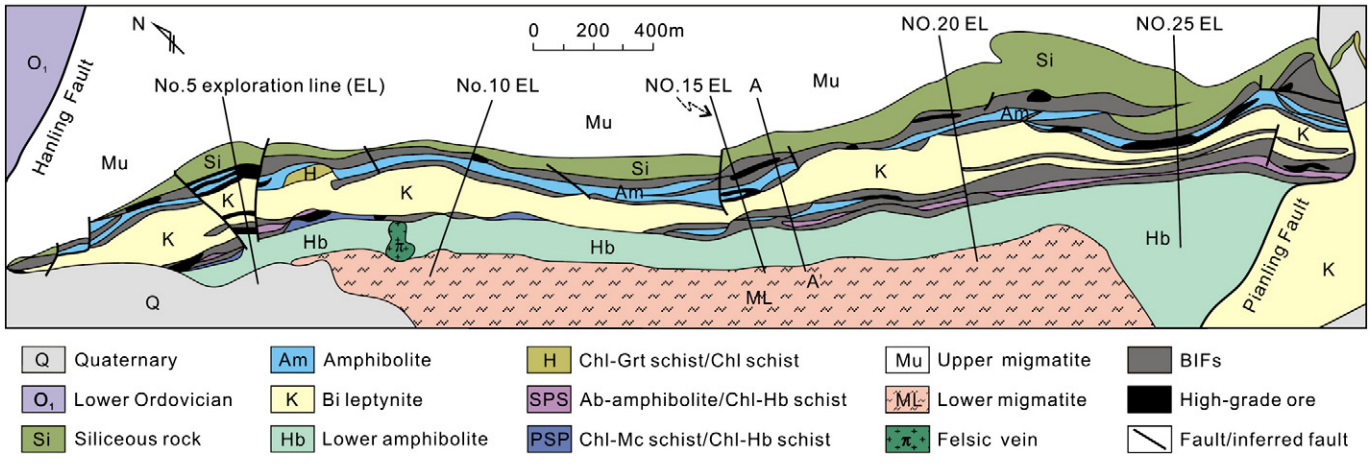

Fig. 2. Geological map of the Gongchangling No. 2 mining area.
Modified after Zhou, 1994.

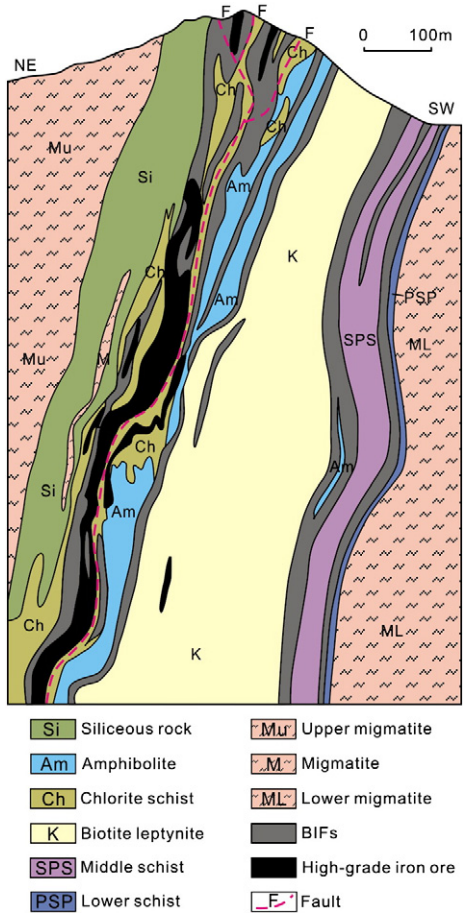

Fig. 3. Geological cross-section (A–A′ in Fig. 2) of the Gongchangling No. 2 mining area. After Chen et al., 1985; Chi, 1993; Zhou, 1994.

the amphibolite samples were from the interlayer of BIFs. All samples used in this study were fresh without visible weathering.

Major oxide analysis was completed at the ALS Chemex (Guangzhou) Co., Ltd. For the major elements, SiO_2, TiO_2, Al_2O_3, $Fe_2O_3^T$, MgO, MnO, CaO, Na_2O, K_2O and P_2O_5 were determined using a PANalytical Axios X-ray Fluorescence spectrometer (XRF) on fused glass beads, and the FeO was determined by wet chemical method. The analytical uncertainty is less than 5%. Trace elements (including rare earth elements) were determined by inductively coupled plasma mass spectrometer (ICP-MS) at the Institute of Geochemistry, Chinese Academy of Sciences in Guiyang, with analytical precision better than 10% RSD. We used standards OU-6, AMH-1 and GBPG-1 as reference materials. The procedure for the trace elements is described in detail by Qi and Gregoire (2000). Mineral chemistry was determined by wavelength-dispersive X-ray emission spectrometry using an EPMA-1600 electron microprobe at the Institute of Geochemistry, Chinese Academy of Sciences. The analytical conditions were as follows: beam current of 10 nA, acceleration voltage of 25 kV and a beam size of 10 μm in diameter. The detection limit for the analyzing elements under such conditions is 0.01%, and the analytical reproducibility is within 2%. The counting time was 20–40 s for major elements and 40–60 s for minor elements. SPI mineral standards (USA) were used for calibration.

4. Results

4.1. Petrology and mineral chemistry

The BIFs are mainly composed of black bands (magnetite-rich bands) alternating with white bands (quartz-rich bands) (Fig. 4a). The black bands are essentially composed of magnetite and less abundant microcrystalline quartz, while the white bands mainly consist of quartz, minor actinolite and magnetite (Fig. 4b). The high-grade iron ore mainly consist of magnetite (Fig. 4c), and the gangue minerals including quartz, cummingtonite, actinolite, garnet, chlorite and calcite (Zhou, 1994). The mineralogy of garnet–chlorite schist mainly consists of garnet and chlorite, showing porphyroblastic texture (Fig. 4d,e). The amphibolite displays medium-fine grained texture, and the main diagnostic metamorphic minerals are hornblende and plagioclase (Fig. 4f).

4.1.1. Magnetite

Magnetite is the main Fe-oxide mineral component of BIFs, magnetite in the magnetite-rich band occurs as both individual grains and aggregates, while it was found as individual grains and inclusions in the quartz-rich band. In both units, magnetite occurs as anhedral to subhedral grain ranging from 0.02 mm to 0.3 mm in size (Fig. 4a,b). Magnetite is also the main Fe-oxide mineral component of massive ore (high-grade iron ore) which mainly consists of euhedral to subhedral magnetite grain with the size varying from 0.1 mm to 0.8 mm (Fig. 4c).

The magnetites in the magnetite-rich band, quartz-rich band and massive ore exhibit the similar chemical component, and are quite different from those of magmatic, skarn and sedimentary type ore deposits (Chen et al., 1984). However, magnetite in quartz-rich band is slightly richer in SiO_2 and Na_2O, while magnetite in magnetite-rich band and massive ore is relatively richer in Al_2O_3, and variable poor in SiO_2 (Fig. 5a).

4.1.2. Quartz

Quartz is euhedral or subhedral, occurring as fine or micro grained size (0.02–0.2 mm). Quartz is one of the main components in the BIFs, mainly occurring as both aggregates with equiangular triple points in quartz-rich band and individual grain in magnetite-rich band (Fig. 4a, b). Quartz in quartz-rich band with straight to curve boundaries commonly shows granoblastic texture.

In chemical composition, the quartz in the magnetite-rich band is slightly richer in FeO and Cr_2O_3 than those in quartz-rich band (Fig. 5b).

4.1.3. Garnet

Garnet is mainly distributed in the altered wall-rocks and minor in the ore samples, and it is more widely distributed in the upper iron belt than in the lower belt. The grain size of garnet in the lower iron belt and middle leptynite mainly ranges from 0.2 mm to 1.0 mm, whereas in the upper iron belt it is much coarser, the maximum size reaches up to 15 cm (Zhou, 1994). The garnet in this study is from garnet–chlorite schist which is the altered hosting rock of high-grade iron ore of upper iron belt and occurs as layered bed. The garnet is present in schist as euhedral, rhombic dodecahedron porphyroblast about 2 cm in size, surrounded by the matrix mineral of chlorite (Fig. 4d,e). The garnet contains mineral inclusions of magnetite and quartz with developed crack. Chlorite is the altered product of garnet, occurring at dense fissure areas. We made a chemical composition profile across garnet from rim through core to rim (Fig. 4e), avoiding inclusions and altered minerals.

With respect to end member, the garnet is dominated by almandite (0.884–0.929), with minor pyrope (0.047–0.079), spessartite (0.002–0.046) and andradite (0.004–0.026), and high XFe values which vary between 0.921 and 0.950 (see Supplementary data). The garnet exhibits pronounced compositional zoning and can be summarized as (1) the content of MnO gradually decreases from the core to the rim, and (2) MgO gradually increases from the core to the rim (Fig. 6).

4.1.4. Hornblende

Amphibolite mainly consists of hornblende and plagioclase (Fig. 4f). The amphibolite in this study is from interlayer of BIFs in the upper iron belt. The hornblende is euhedral to subhedral, fine grained columnar crystal, showing strong pleochroism and oriented arrangement.

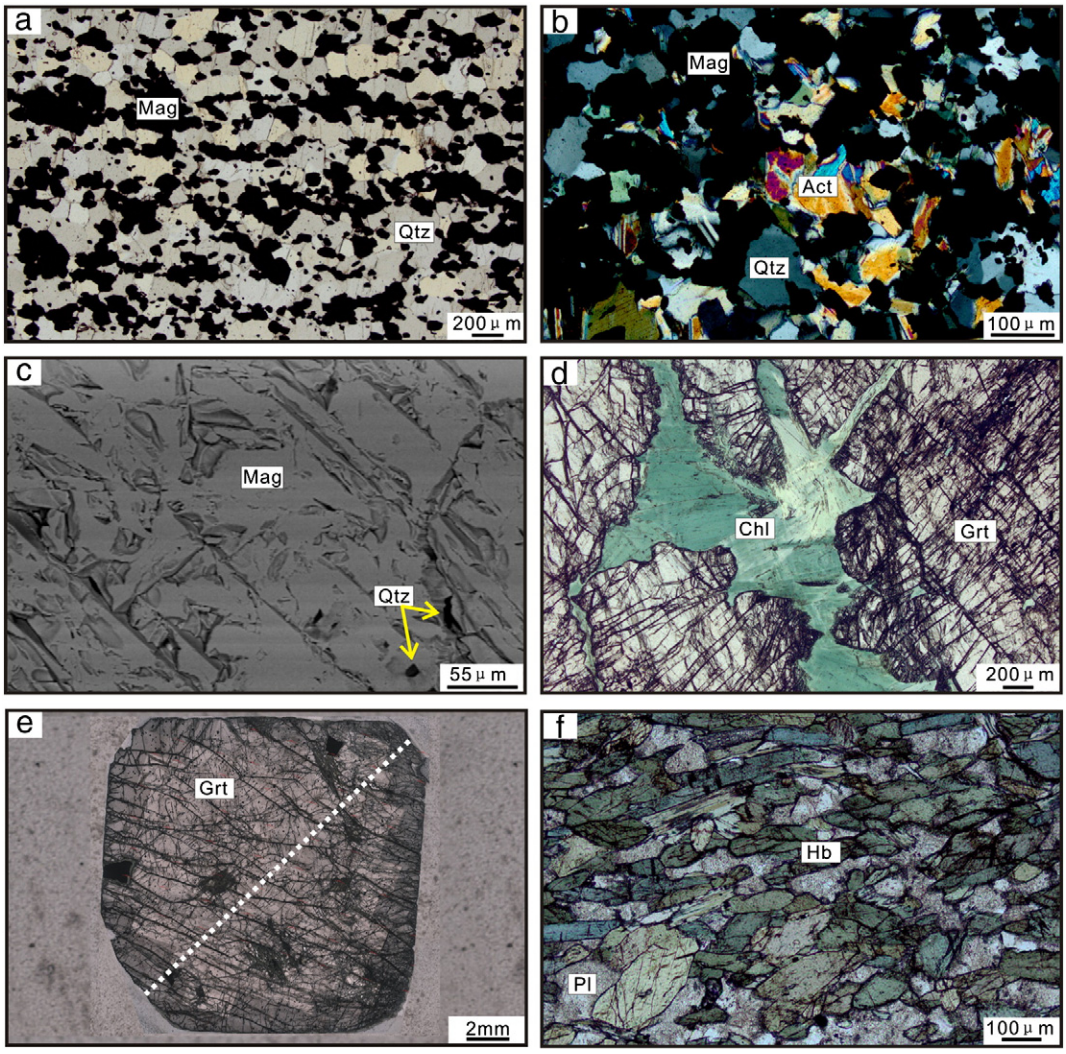

Fig. 4. Photomicrographs showing the representative mineral assemblage and texture of iron ore and wall-rock from the Gongchangling No. 2 mining area. (a) Magnetite-rich (Mag) bands alternating with quartz-rich (Qtz) bands (plane-polarized light; PO-1); (b) Actinolite (Act) in BIFs (crossed polarized light; PO-4); (c) coarse magnetite in high-grade iron ore (BSE; RO-2); (d) garnet-chlorite schist consisting of garnet (Grt) and chlorite (Chl), showing porphyroblastic texture (plane-polarized light); (e) euhedral garnet from garnet–chlorite schist (plane-polarized light); (f) amphibolite consisting of fine grained hornblende (Hb) and plagioclase (Pl) (plane-polarized light).

The calculation of crystal–chemical formulas of hornblende shows the following characteristics: $(Ca + Na)_B = 1.868–1.975$ (≥ 1.00); $Na_B = 0.029–0.150$ (<0.50); $Ca_B = 1.718–1.946$ (≥ 1.50); $(Na + K)_A = 0.230–0.398$ (<0.50); $Ca_A < 0.5$; $Si^T = 6.680–7.203$; $Mg / (Mg + Fe^{2+}) = 0.604–0.725$ (Table 1). According to the International Mineralogical Association's approved amphibole nomenclature (Leake et al., 1997), the hornblende is a member of the calcic group. Calcic amphibole widely occurred in the metamorphic rocks of different metamorphic grades, and there is a close relationship between Ti, Al^{IV}, Na + K contents of amphibole and metamorphic temperature. Based on the discriminate diagrams proposed by Jin (1991), the hornblendes were formed during lower amphibolite facies metamorphism (Fig. 7).

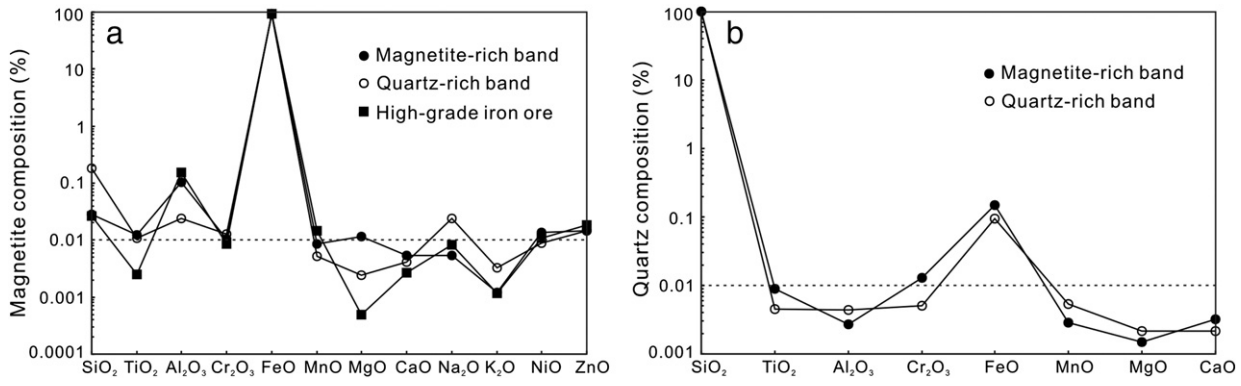

Fig. 5. The average contents of main constitute in magnetite and quartz from different bands and ore types.

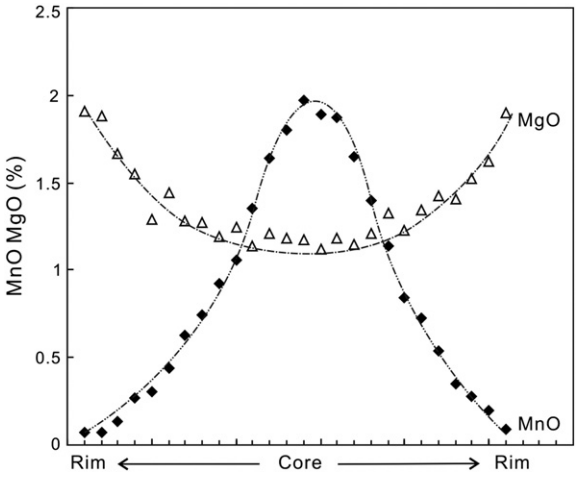

Fig. 6. The compositional profile of garnet.

4.1.5. Plagioclase

The plagioclase coexisting with hornblende is subhedral to anhedral, fine grained, occurring as columnar and tabular crystal (Fig. 4f). Some plagioclase grains suffered slight alteration.

The plagioclase is dominated by oligoclase compositions (An = 20.9%–28.8%) and relatively homogeneous in chemical composition (see Table 1).

4.2. Whole rock geochemistry of iron ore

4.2.1. Major elements

The major element compositions of ten ore samples including five BIFs and five high-grade iron ore samples are listed in Table 2. Fe and Si are the main components, with $Fe_2O_3^T$ and SiO_2 combined representing 93 to 100% of the sample, and there is a strong negative relationship between $Fe_2O_3^T$ and SiO_2. The contents of Al_2O_3 and TiO_2 in all ore samples are low (Al_2O_3 = 0.05–0.87% and TiO_2 = <0.01–0.02%). The Fe^{3+} / ($Fe^{3+}+Fe^{2+}$) ratios for all ore samples range from 0.63 to 0.67 which approach the ratio of 0.67 for pure magnetite except for PO-4 of 0.52, indicating that magnetite is the major ore mineral.

4.2.2. Trace and rare earth elements

The whole-rock trace and rare earth element (REE) concentrations of BIFs and high-grade iron ore samples are presented in Table 2. Yttrium shows the similar chemical behavior to REE, so that it was inserted between Dy and Ho based on its ionic radius (Bau et al., 1996). The REY (REE + Y) for all ore samples are normalized to the post-Archean Australian shale (PAAS, subscript SN, McLennan, 1989), North American shale composite (NASC, subscript NN, Gromet et al., 1984) and Chondrite (CI, subscript CN, Sun and McDonough, 1989). La, Ce, Gd and Y anomalies are defined as follows: $La/La^* = La_N / (3Pr_N - 2Nd_N)$, $Ce/Ce^* = Ce_N / (2Pr_N - Nd_N)$, $Gd/Gd^* = Gd_N / (2Tb_N - Dy_N)$, and Y anomalies assessed using the Y/Ho ratio (higher or lower than 26), respectively (Bolhar et al., 2004). Whereas, Eu anomaly is defined as $Eu/Eu^* = Eu_N / (0.67Sm_N + 0.33Tb_N)$ following Bau and Dulski (1996). The fractionations of LREE/HREE and MREE/HREE were expressed as $(Nd/Yb)_N$ owing to the La and Ce anomalies in seawater and $(Sm/Yb)_N$, respectively. The $(Ce/Ce^*)_{SN} - (Pr/Pr^*)_{SN}$ plot introduced by Bau and Dulski (1996) was used to discriminate the real La and Ce anomalies in BIFs for anomalous abundances of La, and the $(Ce/Ce^*)_{SN}$ and $(Pr/Pr^*)_{SN}$ ratios are calculated as $Ce_{SN} / (0.5La_{SN} + 0.5Pr_{SN})$ and $Pr_{SN} / (0.5Ce_{SN} + 0.5Nd_{SN})$, respectively.

The concentrations of trace elements including transition trace metals, high field strength elements (HFSE), large ion lithophile elements (LILE) and REE are relatively lower compared to the Archean Upper Crust composition (Fig. 8). Crustal contamination is excluded for the low concentration of HFSE (Th, Zr, Hf and Sc) which are normally enriched in evolved crust.

The PAAS normalized REY patterns are consistent for all BIFs and high-grade iron ores samples and show the following characteristics: i) LREE depletion relative to HREE (Nd_{SN}/Yb_{SN} = 0.16–0.80 for BIFs and 0.15–0.47 for high-grade iron ore, respectively) and depletion MREE relative to HREE (Sm_{SN}/Yb_{SN} = 0.22–0.71 for BIFs and 0.12–0.46 for high-grade iron ore, respectively); ii) a slightly positive or no Ce anomaly (Ce_{SN}/Ce_{SN}^* = 1.05–1.45 for BIFs and 0.97–1.71 for high-grade iron ore, respectively); and iii) positive La anomalies (La_{SN}/La_{SN}^* = 1.18–4.06 for BIFs and 1.21–1.92 for high-grade iron ore except RO-4 with extremely high value of 7.78, respectively); iv) positive Eu anomalies (Eu_{SN}/Eu_{SN}^* = 1.55–3.09 for BIFs and 0.97–3.69 for high-grade iron ore, respectively), v) slightly positive Gd anomalies (Gd_{SN}/Gd_{SN}^* = 1.02–1.23 for BIFs and 1.03–1.52 for high-grade iron ore, respectively); and vi) positive Y anomalies (Y/Ho = 34–52 for BIFs and 40–47 for high-grade iron ore, respectively) (Fig. 9).

5. Discussion

5.1. Constraints on the source of ore-forming material

5.1.1. Contamination and mobility on REY

REEs are particularly useful as geochemical tracers (Chen et al., 1991, 1992, 1994, 1996; Taylor and McLennan, 1985; Wang et al., 1989). BIFs, as Precambrian chemical sediments, their REY features might be affected by the syndepositional contamination of terrestrial material and post-depositional diagenesis and metamorphism (Chen, 1996; Tang et al., 2009a, 2013b). Aluminum and titanium are considered to be generally immobile during hydrothermal, diagenetic and weathering processes, and the contents of them may give some constraints on origins and depositional positions of sedimentary rocks (Kato et al., 1996). Moreover, the terrigenous clastic sediments are generally high in the contents of Al_2O_3 and TiO_2 (Lascelles, 2007; Tang et al., 2009a, 2013b). As to the contamination, the low contents of Al_2O_3, TiO_2 and HFSE indicate that little crustal clastic material was involved in the genesis of the Gongchangling iron deposit. Moreover, terrestrial material (common igneous rocks and epiclastic sediments) has a constant chondritic Y/Ho weight-ratio of 28, whereas the Y/Ho ratio of modern seawater displays a superchondritic Y/Ho ratio (>44) (Bau and Dulski, 1999; Nozaki et al., 1997). Therefore, a small mixture of terrestrial material to chemical precipitate from seawater would result in the decrease of seawater-like Y/Ho ratio and cause co-variation between Y/Ho ratio and lithophile elements such as Zr, Th and Hf. The poor correlations between Y/Ho with Zr, Th and Hf contents indicate that the amount of detrital contaminants was trivial. With respect to the influence of post-depositional processes, the previous studies have suggested that REY could not be mobilized during diagenesis, and detritus-free BIFs in different areas display similar REY patterns regardless of metamorphic grade, indicating that diagenesis and metamorphism has little effect on the REY features of BIFs on the whole (Bau, 1991; Bau and Möller, 1993). In summary, the addition of terrestrial material to the iron ores may be little, and the post-depositional process may not disturb the REY patterns. Therefore, we consider that the REY patterns observed in the Gongchangling iron ore samples were the primitive features of detritus-free chemical precipitates.

5.1.2. Source of iron

The seawater inheritance can be recognized from the REY pattern of slight LREE depletion and HREE enrichment, with positive La, Gd, Y anomalies and negative Ce anomaly (Bolhar et al., 2004). A negative Ce anomaly of seawater arises from oxidation of Ce^{3+} to Ce^{4+} and subsequently decouples of Ce from other trivalent REE due to formation of less soluble Ce^{4+} species and/or preferential adsorption of Ce^{4+} species onto particle surfaces (Alibo and Nozaki, 1999; Basta et al., 2011; Byrne

Table 1
Representative composition of hornblende and plagioclase.

Sample (%)	Hornblende									Sample (%)	Plagioclase								
	Hb-1	Hb-2	Hb-3	Hb-4	Hb-5	Hb-6	Hb-7	Hb-8	Hb-9		Pl-1	Pl-2	Pl-3	Pl-4	Pl-5	Pl-6	Pl-7	Pl-8	Pl-9
SiO_2	45.99	48.98	48.05	47.85	47.76	44.81	47.14	46.05	45.15	SiO_2	61.10	61.70	61.19	59.90	60.89	60.22	61.01	60.26	59.40
TiO_2	0.371	0.382	0.348	0.275	0.283	0.518	0.410	0.433	0.532	TiO_2	0.017	0.004	0.007	0.000	0.010	0.012	0.003	0.000	0.013
Al_2O_3	8.024	7.606	8.235	8.017	8.239	11.36	9.654	10.28	10.77	Al_2O_3	24.45	24.17	24.82	23.55	24.45	23.88	24.69	24.75	23.87
Cr_2O_3	0.047	0.018	0.067	0.044	0.077	0.040	0.040	0.057	0.041	Cr_2O_3	0.000	0.020	0.010	0.000	0.000	0.000	0.000	0.004	0.010
FeO	14.42	12.00	13.23	12.74	12.46	14.25	12.95	13.44	14.58	FeO	0.158	0.155	0.142	0.467	0.158	0.889	0.156	0.186	0.585
MnO	0.292	0.288	0.343	0.285	0.318	0.295	0.273	0.303	0.260	MnO	0.003	0.010	0.015	0.000	0.014	0.039	0.000	0.000	0.008
MgO	11.71	13.60	13.37	13.67	13.86	11.32	12.68	12.34	11.45	MgO	0.004	0.017	0.000	0.161	0.000	0.499	0.010	0.013	0.272
CaO	11.93	11.89	11.99	11.72	11.64	11.63	12.09	10.80	11.42	CaO	5.503	4.932	5.739	4.139	5.901	4.721	5.971	5.043	4.319
Na_2O	1.256	0.965	1.142	1.131	0.964	1.388	1.214	1.263	1.141	Na_2O	8.553	8.434	8.647	7.728	8.407	8.253	8.121	8.293	8.464
K_2O	0.288	0.216	0.241	0.151	0.245	0.334	0.171	0.242	0.314	K_2O	0.057	0.098	0.043	1.147	0.029	0.408	0.031	0.625	0.855
Total	94.32	95.95	97.02	95.88	95.84	95.94	96.61	95.20	95.65	Total	99.85	99.54	100.62	97.09	99.86	98.92	99.99	99.17	97.80
Si	7.005	7.203	7.022	7.042	7.011	6.680	6.924	6.839	6.732	Si	2.717	2.744	2.704	2.740	2.711	2.708	2.709	2.703	2.707
^{IV}Al	0.995	0.797	0.978	0.958	0.989	1.320	1.076	1.161	1.268	Ti	0.001	0.000	0.000	0.000	0.000	0.000	0.000	0.000	0.000
Sum T	8.000	8.000	8.000	8.000	8.000	8.000	8.000	8.000	8.000	Al	1.282	1.267	1.293	1.270	1.283	1.266	1.292	1.308	1.282
^{VI}Al	0.445	0.521	0.440	0.433	0.436	0.675	0.595	0.637	0.624	Cr	0.000	0.001	0.000	0.000	0.000	0.000	0.000	0.000	0.000
Cr	0.006	0.002	0.008	0.005	0.009	0.005	0.005	0.007	0.005	Fe^{3+}	0.006	0.006	0.005	0.018	0.006	0.033	0.006	0.007	0.022
Ti	0.043	0.042	0.038	0.030	0.031	0.058	0.045	0.048	0.060	Fe^{2+}	0.000	0.000	0.000	0.000	0.000	0.000	0.000	0.000	0.000
Fe^{3+}	0.090	0.008	0.216	0.269	0.341	0.212	0.113	0.311	0.319	Mn	0.000	0.000	0.001	0.000	0.001	0.001	0.000	0.000	0.000
Mg	2.658	2.981	2.912	2.999	3.033	2.515	2.776	2.733	2.544	Mg	0.000	0.001	0.000	0.011	0.000	0.033	0.001	0.001	0.018
Fe^{2+}	1.746	1.446	1.386	1.263	1.149	1.535	1.466	1.264	1.449	Ca	0.262	0.235	0.272	0.203	0.281	0.227	0.284	0.242	0.211
Mn	0.013	0.000	0.000	0.000	0.000	0.000	0.000	0.000	0.000	Na	0.738	0.727	0.741	0.685	0.726	0.720	0.699	0.721	0.748
Sum C	5.000	5.000	5.000	5.000	5.000	5.000	5.000	5.000	5.000	K	0.003	0.006	0.002	0.067	0.002	0.023	0.002	0.036	0.050
Mg	0.000	0.000	0.000	0.000	0.000	0.000	0.000	0.000	0.000	Total	5.009	4.986	5.018	4.993	5.008	5.013	4.992	5.018	5.039
Fe^{2+}	0.000	0.023	0.014	0.035	0.040	0.030	0.012	0.094	0.050										
Mn	0.025	0.036	0.042	0.036	0.040	0.037	0.034	0.038	0.033	An	26.14	24.28	26.77	21.24	27.90	23.44	28.84	24.25	20.91
Ca	1.946	1.874	1.878	1.848	1.830	1.857	1.902	1.718	1.824	Ab	73.53	75.14	72.99	71.75	71.93	74.15	70.98	72.17	74.16
Na	0.029	0.067	0.065	0.081	0.090	0.076	0.052	0.150	0.094	Or	0.322	0.575	0.239	7.007	0.163	2.412	0.178	3.579	4.929
Sum B	2.000	2.000	2.000	2.000	2.000	2.000	2.000	2.000	2.000										
Na	0.342	0.208	0.258	0.242	0.184	0.325	0.293	0.214	0.236	T(°C)	539	520	577	571	595	579	551	594	576
K	0.056	0.041	0.045	0.028	0.046	0.064	0.032	0.046	0.060										
Sum A	0.398	0.248	0.303	0.270	0.230	0.388	0.325	0.260	0.296										
Total	15.40	15.25	15.30	15.27	15.23	15.39	15.33	15.26	15.30										

The amount of Fe^{3+} was calculated from stoichiometric constraints using program AX (Powell et al., 1998). The temperature (T) was calculated based on the amphibole-plagioclase thermometry proposed by Holland and Blundy (1994).

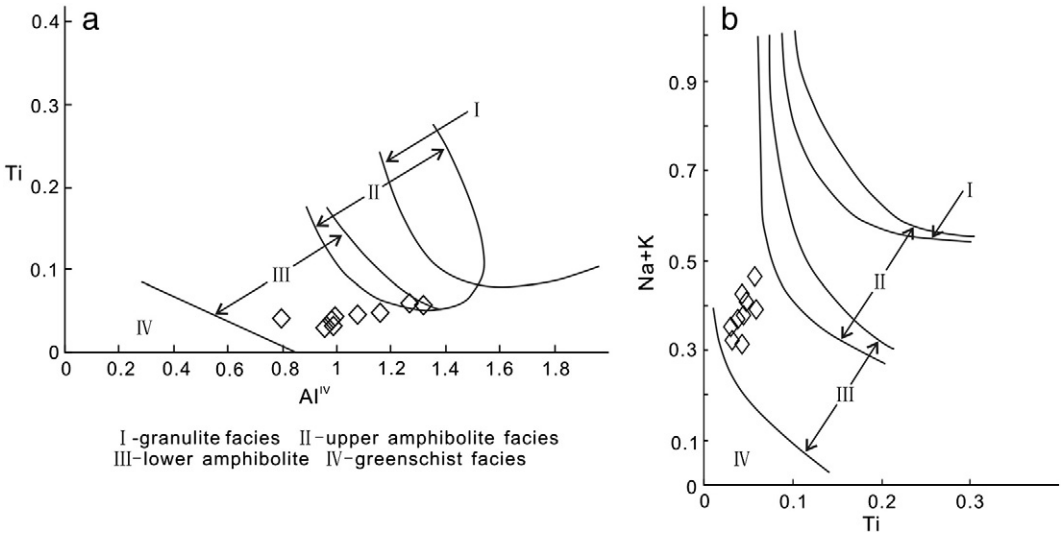

Fig. 7. The Al^{IV}–Ti and Ti–(Na + K) metamorphic facies discrimination diagrams of amphibole. After Jin, 1991.

and Kim, 1990; Chen and Fu, 1991; Chen and Zhao, 1997). The REY patterns of all ore samples including BIFs and high-grade iron ores show the LREE and MREE relative to HREE depletion characteristics, with positive La, Gd and Y anomalies. However, unlike the modern seawater in which the obvious negative Ce anomaly is observed, according to Fig. 10, the ore samples mainly show a lack of negative Ce anomalies, suggesting that the Archean fO_2 was much lower than that of modern seawater. All the ore samples exhibit strong seawater signatures except Ce and Eu anomalies, and indicate that the seawater contributes to the genesis of the Gongchangling iron deposit.

The seawater does not show positive Eu anomaly, whereas the high-temperature hydrothermal solution is characterized by LREE-enriched pattern with positive Eu anomaly (Bau and Dulski, 1999; Danielson et al., 1992). The ore samples exhibit obviously positive Eu anomaly, suggesting that the hydrothermal fluid is also involved in the genesis of the Gongchangling iron deposit. Huston and Logan (2004) proposed that systematic differences in the intensity of Eu anomaly exist between Algoma type and Superior type BIFs, and the Algoma type BIFs are characterized by much larger Eu_{NN} (normalized to NASC) anomaly (>1.8) than Superior type BIFs (<1.8). The ore samples show the much larger Eu_{NN} anomaly (average of 2.4 for all samples, Table 2), indicating that the Gongchangling iron deposit is an Algoma type BIFs related to submarine volcanic hydrothermal activity. According to Bau and Dulski (1996), the high temperature hydrothermal fluids (>250 °C) which typically developed at mid-ocean ridges and back-arc spreading centers exhibit highly positive Eu_{CN} anomalies (normalized to Chondrite), whereas the low temperature hydrothermal fluids (<250 °C) characterize no or weak Eu_{CN} anomalies. The Eu_{CN} anomalies of all ore samples (Table 2) show moderately positive Eu_{CN} anomalies (average of 1.6), and indicate that the high temperature hydrothermal fluid is associated with the formation of the Gongchangling iron deposit.

The Al_2O_3–SiO_2 discrimination diagram was used to discriminate the origin of ferro-manganiferous rocks (Gonzalez et al., 2009; Wonder et al., 1988). The ore samples were mainly plot in the hydrothermal field, and some within hydrogenous field due to the less contents of SiO_2 (Fig. 11). Since hydrothermal fluids have a chondritic Y/Ho ratio (28), while that of modern seawater is superchondritic (>44) (Bau and Dulski, 1999), the average Y/Ho ratios of all ore samples (41) is slightly less than 44, it is reasonable to infer that the iron ores were chemical precipitate from the mixture of seawater and hydrothermal fluids. Conservative two end-member mixing calculation indicates that Eu/Sm ratios of the Gongchangling iron ores could be accounted by a high temperature hydrothermal fluid of ca. 0.1% mixing with seawater (Fig. 12a). Moreover, a less than 1.0% contribution of high temperature hydrothermal fluid may also account for the Sm/Yb ratios observed in the ore samples (Fig. 12b), which generally match up with the maxing ratio to account for Eu/Sm ratio (Fig. 12c; Alexander et al., 2008; Bau and Möller, 1993; Tang et al., 2013b). This is comparable with the model of 1000:1 mixing ratio of seawater and hydrothermal fluid to explain the REY distribution in BIFs (Khan et al., 1996; Klein and Beukes, 1989).

In conclusion, the REY patterns and element ratios of ore samples show the characteristics of both seawater and hydrothermal fluid. The positive Eu anomalies in the iron ores indicate that the high-temperature hydrothermal alteration of the oceanic crust plays an important role in the BIFs' deposition. Therefore, we propose that the Gongchangling iron deposit was formed in a submarine volcanic environment, and the mixture of seawater and hydrothermal fluid which percolated and dissolved the submarine volcanic rock (seafloor basalts or mafic rocks) supplied the ore-forming material.

5.2. Origin of BIFs and its tectonic implications

5.2.1. Origin and tectonic setting of the Gongchangling BIFs

The Neoarchean is an important continent-formation period of the Earth with two peaks of ca. 2.7 Ga and ca. 2.5 Ga according to the Nd isotope distribution (Condie et al., 2009). The 2.7 Ga tectonic-thermal events are widely developed in many cratons around the world, whereas the 2.5 Ga tectonic-thermal events have been identified only in a few cratons including the NCC (Wan et al., 2011). The early Neoarchean (2.75–2.70 Ga) tectonic–thermal events might have been well developed in the NCC, however, the NCC is better known for the strong tectonic–thermal events at the late Neoarchean (2.55–2.5 Ga), with supracrustal rock formation, magmatism and metamorphism all over the NCC (Wan et al., 2012a). As to the 2.5 Ga tectonic–thermal events in the NCC, the cause and nature have been hotly debated, with one school of thought arguing for a magmatic arc model (Kröner et al., 2005; Kusky et al., 2001; Wan et al., 2012a,b; Wilde et al., 2005). Whereas another school proposed magma underplating caused by the mantle model to explain it (Geng et al., 2006; Grant et al., 2009; Yang et al., 2008; Zhao, 2009; Zhao et al., 1998).

The BIFs in the NCC occur not only in greenstone belts (GB) but also in high-grade regions (HR) (Zhai and Windley, 1990). Zhai and Santosh (2011) suggested that most of the GB in the NCC which show an age range of ca. 2.54–2.6 Ga were formed in an island arc or a back-arc basin setting, and the GB represent the vestiges of older arc–continent

Table 2
Major, trace and REE analysis of BIFs and high-grade iron ores from the No. 13 exploration tunnel of the Gongchangling No. 2 mining area.

Ore type sample	BIFs					High-grade iron ores				
	PO-1	PO-2	PO-3	PO-4	PO-5	RO-1	RO-2	RO-3	RO-4	RO-5
Major oxides (%)										
SiO_2	56.92	51.01	36.22	41.48	52.20	3.18	1.60	0.47	1.14	1.41
TiO_2	<0.01	<0.01	<0.01	0.02	<0.01	<0.01	<0.01	<0.01	<0.01	<0.01
Al_2O_3	0.23	0.20	0.16	0.87	0.25	0.54	0.34	0.21	0.05	0.05
$Fe_2O_3^T$	42.69	48.99	57.38	53.80	48.61	96.55	98.79	99.97	97.83	96.88
MnO	0.02	0.03	0.11	0.09	0.04	0.12	0.09	0.06	0.12	0.12
MgO	0.21	0.16	1.47	2.03	0.23	0.51	0.41	0.06	0.11	0.13
CaO	0.14	0.04	3.21	2.09	0.01	0.03	<0.01	0.35	0.01	0.01
Na_2O	<0.01	<0.01	0.03	0.11	<0.01	0.03	0.06	0.02	0.02	0.02
K_2O	<0.01	<0.01	0.03	0.07	<0.01	0.01	<0.01	0.01	0.01	<0.01
P_2O_5	0.092	0.009	0.124	0.132	0.001	0.005	0.012	<0.001	<0.001	<0.001
LOI	−1.07	−1.40	0.66	−1.33	−1.42	−2.61	−2.44	−2.56	−0.74	−0.29
Total	99.23	99.04	99.39	99.36	99.92	98.37	98.86	98.59	98.55	98.33
FeO	13.05	15.50	19.20	23.20	15.35	30.70	30.50	30.00	29.90	30.20
XFe^{3+}	0.66	0.65	0.63	0.52	0.65	0.65	0.66	0.67	0.66	0.65
Trace and REE elements (ppm)										
Ni	1.91	1.26	0.20	5.32	1.17	11.0	13.8	26.3	15.0	15.6
Cr	15.0	12.7	15.1	25.2	12.0	20.9	21.9	23.0	22.1	21.8
V	3.47	1.42	2.01	14.6	1.35	1.71	2.32	1.29	1.01	1.06
Rb	0.422	0.564	7.44	10.6	0.371	2.31	0.980	1.19	0.535	0.523
Sr	2.29	1.83	14.8	22.0	0.883	2.08	1.22	3.44	1.21	1.11
Zr	1.33	0.572	1.04	7.37	1.42	0.898	0.588	0.678	0.469	0.588
Ba	0.815	0.731	3.83	8.26	0.184	1.11	0.239	0.788	0.054	0.207
Th	0.054	0.035	0.042	0.707	0.077	0.094	0.010	0.008	0.006	0.009
U	0.231	0.106	0.093	0.179	0.102	0.257	0.504	0.126	0.425	0.676
Y	2.38	2.44	6.60	7.35	3.18	2.40	5.91	0.718	2.55	3.93
La	0.552	0.356	7.49	3.56	1.27	1.23	1.60	0.266	0.390	1.23
Ce	1.13	0.613	12.0	6.97	2.07	2.03	2.64	0.376	0.674	1.85
Pr	0.142	0.070	1.21	0.773	0.223	0.229	0.299	0.041	0.076	0.200
Nd	0.755	0.335	4.59	3.11	0.914	0.868	1.23	0.166	0.415	0.868
Sm	0.170	0.079	0.670	0.598	0.171	0.139	0.288	0.023	0.093	0.157
Eu	0.111	0.034	0.369	0.436	0.119	0.092	0.070	0.013	0.085	0.146
Gd	0.242	0.138	0.945	0.847	0.280	0.256	0.463	0.051	0.164	0.282
Tb	0.036	0.025	0.118	0.137	0.049	0.036	0.077	0.008	0.027	0.041
Dy	0.232	0.178	0.650	0.927	0.321	0.232	0.475	0.058	0.223	0.302
Ho	0.065	0.047	0.178	0.219	0.084	0.060	0.129	0.015	0.062	0.092
Er	0.171	0.180	0.536	0.663	0.251	0.148	0.397	0.057	0.177	0.252
Tm	0.029	0.028	0.074	0.098	0.034	0.028	0.061	0.010	0.028	0.039
Yb	0.150	0.179	0.476	0.637	0.259	0.153	0.383	0.095	0.177	0.223
Lu	0.025	0.034	0.080	0.108	0.042	0.025	0.062	0.017	0.030	0.034
Hf	0.034	0.018	0.018	0.178	0.028	0.011	0.014	0.010	0.007	0.007
Y/Ho	37	52	37	34	38	40	46	47	41	43
$(Nd/Yb)_{SN}$	0.42	0.16	0.80	0.41	0.29	0.47	0.27	0.15	0.20	0.32
$(Sm/Yb)_{SN}$	0.57	0.22	0.71	0.48	0.34	0.46	0.38	0.12	0.27	0.36
$(La/La^*)_{SN}$	4.06	2.44	1.38	1.18	1.52	1.21	1.44	1.63	7.78	1.92
$(Ce/Ce^*)_{SN}$	1.45	1.32	1.08	1.05	1.11	0.97	1.05	1.05	1.71	1.18
$(Gd/Gd^*)_{SN}$	1.16	1.08	1.23	1.17	1.02	1.26	1.03	1.17	1.52	1.42
$(Eu/Eu^*)_{SN}$	2.84	1.55	2.61	3.09	2.65	2.65	0.97	1.83	3.43	3.69
$(Eu/Eu^*)_{NN}$	2.71	1.50	2.48	2.96	2.55	2.55	0.93	1.77	3.30	3.54
$(Eu/Eu^*)_{CN}$	1.79	1.03	1.60	1.96	1.74	1.71	0.63	1.24	2.26	2.39

$Fe_2O_3^T$, total Fe expressed as Fe_2O_3; LOI, Loss on ignition; XFe^{3+}, $Fe^{3+}/(Fe^{2+}+Fe^{3+})$; subscript SN, normalized to post-Archean Australian shale (PAAS); subscript NN, normalized to North American shale composite (NASC); subscript CN, normalized to Chondrite (CI).

collision. However, with respect to the classification of the Gongchangling iron deposit, it is still controversial. Zhai and Windley (1990) proposed that they were HR type BIFs, while they were also considered as the GB type BIFs located in the middle part of the Anshan–Benxi GB (Zhang et al., 2012a). Based on the regional geology, lithologic association, and geochemical features of the associated meta-volcanics and orthogneisses, it was suggested that the HR type of BIFs formed initially in arcs, which were intruded by voluminous tonalites and granodiorites, and later converted by deformation and high-grade metamorphism into orthogneisses, while the GB type of BIFs likely formed in a geological environment similar to rifts or back-arc basins and arcs (Zhai and Santosh, 2013). It suggests that both the HR type and GB type BIFs probably formed in the tectonic setting related to arcs. The Gongchangling iron deposit is a volcanic rock-related Algoma type BIFs based on the mineralogy, rock association and geochemical characteristics (Shen, 1998). Previous studies have suggested that the Gongchangling BIFs were developed on the continental basement (Tiejiashan gneiss) (Zhai and Windley, 1990; Zhai et al., 1990a, b; Zhou, 1994). Moreover, the iron ore samples show the geochemical characteristics of both seawater and hydrothermal fluid. Furthermore, the geochemical study of metasediments and amphibolites which are the hosting rocks of the Gongchangling iron deposit demonstrates that they are formed in an island arc-related tectonic setting (Sun et al., 2014; Wang et al., 2013). Therefore, we prefer to the arc model and infer that the Gongchangling iron deposit was formed in a subduction-related submarine volcanic setting.

5.2.2. Tectonic connection between BIFs deposition and global events

The BIFs are widely distributed in the NCC which is one of the oldest cratons in the world (Liu et al., 1992; Zhang et al., 2012a). The formation age of BIFs in the NCC covers a wide range from the Paleoarchean to the early Paleoproterozic, but the peak period is the late Neoarchean

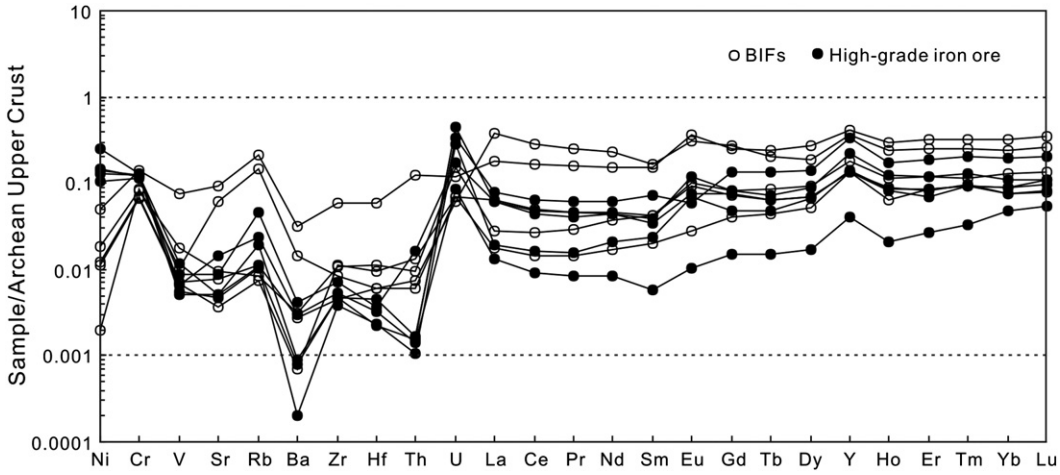

Fig. 8. The Archean Upper Crust-normalized trace and REE diagram. The data of Archean Upper Crust are from Taylor and McLennan (1995).

(2.50–2.55 Ga) (Wan et al., 2012b; Zhang et al., 2012a). The large scale BIFs' mineralization at ca. 2.5 Ga in the NCC may predate to the final amalgamation of the NCC (Zhai, 2010; Zhang et al., 2011). The 2.5 Ga is also the peak time for the genesis of BIFs in other cratons around the world (Bekker et al., 2010; Klein, 2005). Therefore, it is reasonable to infer that there may be a global event leading to the intense formation of BIFs at ca. 2.5 Ga. It is likely that the world-wide BIFs' formation at ca. 2.5 Ga may be in connection with amalgamation of a Neoarchean supercontinent, Kenorland or supercratons of Vaalbara, Superia, and Sclavia (Aspler and Chiarenzelli, 1998; Bleeker, 2003; Bradley, 2011; Rogers and Santosh, 2003; Williams et al., 1991).

The earliest supercontinent Kenorland was firstly proposed by Williams et al. (1991). It was proposed that Kenorland became a continent at ca. 2.5 Ga but then rifted apart into at least three separate regions that were later reassembled into their former positions along two ca. 1.8 Ga orogenic belts (Trans-Hudson and Taltson-Thelon). Zhai et al. (2000) pointed out that the amalgamation of the NCC at ca. 2.5 Ga might have a relationship with the Svecofennides (Northwest Europe), North America and some other ancient continents to form a supercontinent. According to Li et al. (2001), the NCC was an integral part of the Kenorland supercontinent. However, Bleeker (2003) identified at least three supercratons instead of a single supercontinent at late Archean based on common themes among the world's 35 known Archean crustal blocks: Vaalbara, Superia, and Sclavia. The major differences between these three supercratons include the relative age of cratonization, chronology of mafic dyke swarm events, stratigraphy and chronology of Paleoproterozoic cover sequences. According to Bleeker (2003), the Dharwar craton of peninsular Indian, the Zimbabwe craton of southern Africa, and the Wyoming craton of North America all show significant similarities to the Slave craton. It is inferred that at least some of these blocks which were nearest neighbors to the Slave craton formed the ca. 2.6–2.2 Ga Sclavia supercraton. Moreover, Zhao et al. (2003) proposed that the Eastern Block of the NCC and South Indian Block which consists of Dharwar, Bastar and Singbhum cratons were once a single continent from the Archean till Paleoproterozoic era. Consequently, it is reasonable to infer that the NCC may be part of Sclavia supercraton. Therefore, the worldwide distribution of BIFs at ca. 2.5 Ga might provide an important clue to reconstruct the assembly of Kenorland supercontinent or Sclavia supercraton at the Neoarchean era.

5.3. Origin of high-grade iron ore

5.3.1. Metamorphism

Since metamorphic event at Archean/Proterozoic has been recognized across the large tracts of the NCC, it appears to be of wide regional significance (Grant et al., 2009; Yang et al., 2008; Zhang et al., 2011, 2012b). The Anshan Group supracrustal rocks in the Anshan–Benxi area suffered a varying degree of metamorphism. In general, the grade of metamorphism increases from greenschist facies in the west of the area to amphibolite facies in the east, while the retrograde metamorphism decreases from the west to the east (Zhai and Windley, 1990; Zhai et al., 1990a,b; Zhou, 1994).

It was proposed that the garnet bowl-shaped pattern of MgO content and bell-shaped pattern of MnO content are generally interpreted as a growth zoning produced during the prograde metamorphism, while a reversal of above zoning trends of garnet is interpreted as a reflection of retrogressive diffusion (Frost and Tracy, 1991; Spear, 1991; Zhang et al., 2000). Therefore, the garnet from the wall-rock of high-grade iron ore recorded a compositional feature of growth zoning produced during the prograde metamorphism (Fig. 6).

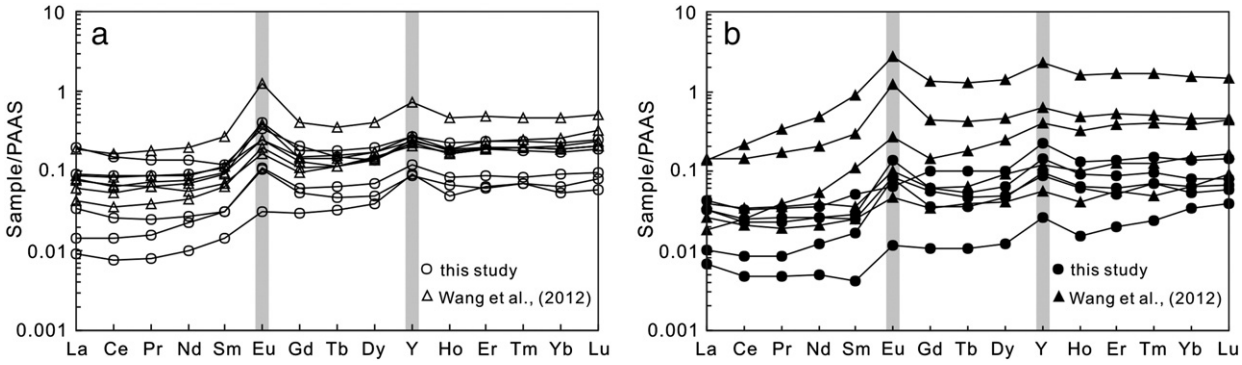

Fig. 9. PAAS-normalized REY patterns of BIFs (a) and high-grade iron ores (b). PAAS values are from McLennan (1989).

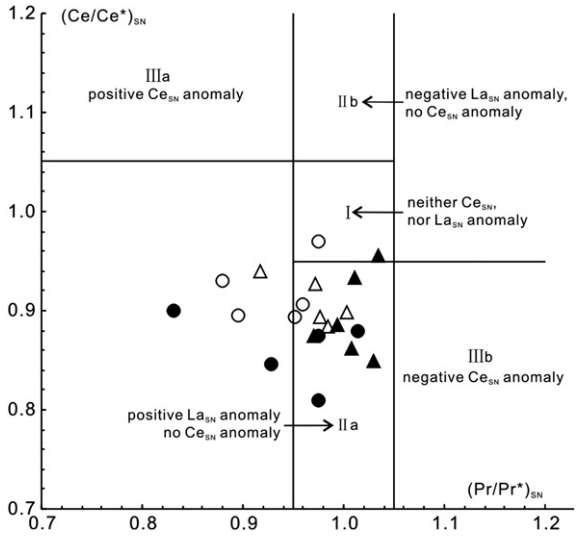

Fig. 10. The $(Ce/Ce^*)_{SN}$ vs $(Pr/Pr^*)_{SN}$ diagram after Bau and Dulski (1996). Symbol illustrations are the same as to Fig. 9.

Due to the ubiquity of amphibole and plagioclase-bearing rocks on the Earth such as granites and amphibolites, Holland and Blundy (1994) proposed an amphibole–plagioclase thermometer for assemblage with or without quartz based on the reactions: edenite + albite = richterite + anorthite. The thermometer would perform well in the range 400–1000 °C and 1–15 kbar over a broad range of bulk compositions. In the Gongchangling No. 2 mining area, amphibolite has a close relationship with BIFs. We applied the thermometer to amphibolites which agree well with the applicable conditions in order to calculate metamorphic temperature. The amphibolite showed a relatively clustering result in the range 520–595 °C with a mean temperature of 567 °C and standard deviation 25 °C for 9 pairs. And according to the chemical composition of hornblende discussed above (Fig. 7), it suggests that the amphibolites were formed during lower amphibolite facies metamorphism.

5.3.2. Genesis of high-grade iron ore

As to the genesis of high-grade iron ore of the Gongchangling No. 2 mining area, it is still one of the unsolved problems which have been hotly debated. The previous studies showed that the occurrence of

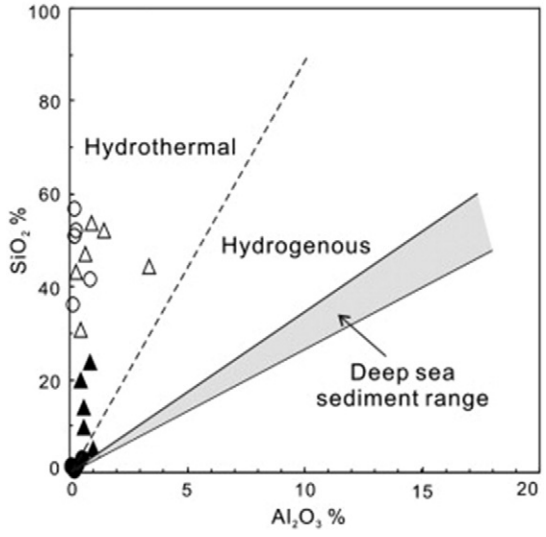

Fig. 11. Diagram to illustrate the origin of primary chemical precipitate based on SiO_2 and Al_2O_3 contents (after Wonder et al., 1988). Symbol illustrations are the same as to Fig. 9.

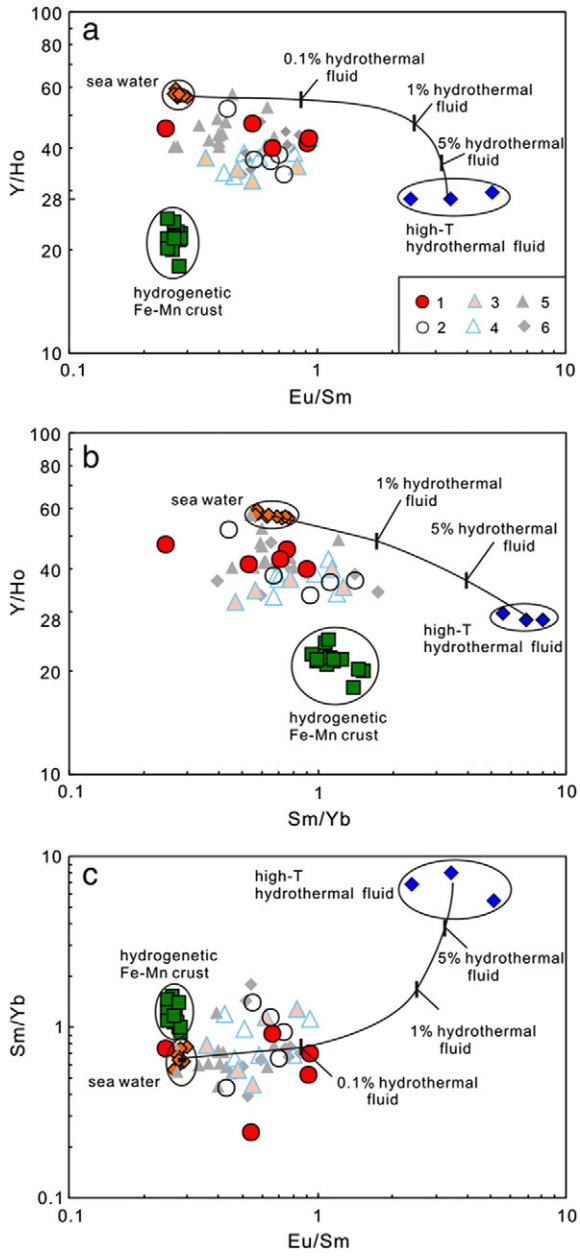

Fig. 12. Elemental ratio plots with two-component conservative mixing lines for Eu/Sm, Sm/Yb, and Y/Ho (after Alexander et al., 2008). 1, high-grade iron ore from this study; 2, BIFs from this study; 3, high-grade iron ore after Wang et al. (2012); 4, BIFs after Wang et al. (2012); 5, 3.7 Ga Isua IF of Greenland after Bolhar et al. (2004); 6, 2.5 Ga Kuruman IF from South Africa (Bau and Dulski, 1996).

high-grade iron ore usually had a close relationship with geological structures, and it usually occurred within or near fault, or within folds' gap (Zhou, 1994). Therefore, the high-grade iron ore might not be the product of original deposition. Siderite decomposition is also not the main way to form high-grade iron ore for the following reasons: i) graphite is not a common mineral in high-grade iron ore; ii) the oxygen isotope composition of magnetite is negative, but the sedimentary siderite generally shows a highly positive value (Liu and Jin., 2010; Zhou, 1994); iii) the carbon isotope compositions of graphite and dolomitic marble which occurred near Fe6 suggest that the graphite may be the decomposition product of marble (Li et al., 2012).

The high-grade iron ores of Gongchangling No. 2 mining area might be formed by hydrothermal reformation. However, the opinions on the nature of hydrothermal fluid were different, and it was argued that the high-grade iron ores were reformed by metamorphic hydrothermal

fluid or migmatitic hydrothermal fluid (Chen et al., 1984; Liu and Jin, 2010; Wang et al., 2012). Previous studies suggested that metamorphic hydrothermal fluid produced during the regional metamorphism stage was rich in iron, and it transferred along the strike reverse fault to form the Gongchangling high-grade iron ores (Guan, 1961; Shi and Li, 1980; Zhou, 1994). The Gongchangling iron deposit is surrounded by the large area of migmatite, and it was also proposed that the migmatitic hydrothermal fluid was involved in the genesis of high-grade iron ores (Chen et al., 1985; Cheng, 1957; Li et al., 1977; Zhao and Li, 1980; Zhao et al., 1979).

Here, combined with previous studies, we prefer to hold that the high-grade iron ore is the reformed product of BIFs by metamorphic hydrothermal fluids with the following evidences:

(1) The occurrence of high-grade iron ore: the high-grade iron ore which shows obvious structural-controlled characteristics usually occurred as layer or vein within BIFs.
(2) Geochemical characteristics: the BIFs and high-grade iron ores show the quite similar geochemical characteristics. The chemical composition of magnetite from BIFs and high-grade iron ore is almost the same, and the REY patterns of BIFs and high-grade iron ores are alike, suggesting little addition of foreign materials. Chemical composition profile of garnet from the wall-rock of high-grade iron ores exhibits a growth zoning produced during the prograde metamorphism. The alkalic compositions of K_2O and/or Na_2O are generally considered that they should be high in migmatitic hydrothermal fluid; however, the contents of K_2O and Na_2O are low in both BIFs and high-grade iron ores, indicating that the role of migmatitic hydrothermal fluid is minor in the genesis of high-grade iron ore.
(3) Fluid inclusions: the study of fluid inclusions suggests that hydrothermal fluid involved in the formation of high-grade iron ore was from local material without the addition of foreign substance (Shi and Li, 1980), indicating that the formation of high-grade iron ore attribute to metamorphic hydrothermal fluid.
(4) Sulfur isotope composition: the sulfur isotope compositions of pyrites from high-grade iron ore show a large range (−5–+14‰) (Chen et al., 1985; Zhou, 1994), suggesting that the high-grade iron ore underwent sulfur isotope fractionation; while the values of BIFs and migmatitic granite are both close to the values of meteorite, consequently, the migmatitic hydrothermal fluid should make the sulfur isotope composition of high-grade iron ore homogenous (Wang et al., 2012; Zhou, 1994). Therefore, migmatitic hydrothermal fluid could not form the high-grade iron ore.
(5) Oxygen isotope composition: the oxygen isotope of magnetite from BIFs shows a large range from −4.41 to +6.16‰, whereas the values of high-grade iron ore are relative low, which varies from −5.4‰ to −0.41‰ (Zhou, 1994). It suggests that the high-grade iron ore was reformed by the fluid rich in light oxygen isotope. However, the oxygen isotope composition of migmatitic hydrothermal fluids generally shows the feature of heavy isotope enrichment (Liu and Jin, 2010). Therefore, the high-grade iron ore should not be the reformed product of BIFs by migmatitic hydrothermal fluid.

Based on the above analysis, we proposed the genetic model of high-grade iron ore. At the late Neoarchean, the Gongchangling BIFs were formed in an arc-related tectonic setting, and then after a short time interval, it suffered lower amphibolite facies metamorphism. The metamorphic hydrothermal fluid from BIFs transferred along weak tectonic zone. When it flowed through BIFs, the fluid would dissolve silicon and carried it away. The magnetite remained and was reformed by metamorphic hydrothermal fluids. As a result, the magnetite enriched and the reformed BIFs became high-grade iron ore.

6. Conclusions

The Gongchangling iron deposit, an oxide facies of Algoma type BIFs located in the Liaoning Province in the NCC, is famous for the production of high-grade iron ores in the Gongchangling No. 2 mining area in China. The petrological and geochemical analysis has led to the following conclusions:

1. The low contents of Al_2O_3, TiO_2 and HFSE in the BIFs and high-grade iron ores indicate that they are detritus-free chemical precipitates. And the post-depositional process may not disturb the REY patterns.
2. The REY patterns and element ratios indicate that both the high-temperature hydrothermal fluid and seawater contribute to the formation of the Gongchangling iron deposit, and it is proposed that the mixture of seawater and hydrothermal fluid which percolated and dissolved the submarine volcanic rocks provided the ore-forming material.
3. It is proposed that the Gongchangling iron deposit was formed in an arc-related tectonic setting at the late Neoarchean, and the worldwide distribution of BIFs at ca. 2.5 Ga might record the assembly of Kenorland supercontinent or Sclavia supercraton.
4. The garnet from the wall-rock of high-grade iron ores exhibits a growth zoning produced during the prograde metamorphism. The amphibolite as the interlayer of BIFs, of which the main mineral assemblages are hornblende and plagioclase, recorded the metamorphic temperature of 567 ± 25 °C, indicating that the iron deposit suffered lower amphibole facies metamorphism.
5. Our data, combined with previous studies, supports that the high-grade iron ore is the reformed product of BIFs by metamorphic hydrothermal fluids. It was proposed that the BIFs suffered lower amphibole facies metamorphism, and the metamorphic hydrothermal fluids flowed through the weak zone within BIFs resulting in the dissolving of silicon and growth of magnetite to form the high-grade iron ore.

Supplementary data to this article can be found online at http://dx.doi.org/10.1016/j.oregeorev.2013.12.017.

Acknowledgments

This research was financially supported by the Major State Basic Research Program of China (No. 2012CB416602), Special Research Fund of State Key Laboratory of Ore Deposit Geochemistry, and the Knowledge Innovation Program of Chinese Academy of Sciences (No. KZCX2-YW-Q04-07). We gratefully acknowledge Prof. Zhong-Gang Wang for the valuable discussion, Dr. Da-Peng Wang and Kai-Wen Li for providing help in the field investigations. The authors also thank Wen-Qin Zheng, Yan Huang, Jing Hu and Guang-Ping Bao for their help in microprobe and trace element analysis. Constructive reviews by two anonymous referees and editorial handling by Prof. Hong-Rui Fan greatly improved the quality of the manuscript.

References

Alexander, B.W., Bau, M., Andersson, P., Dulski, P., 2008. Continentally-derived solutes in shallow Archean seawater: rare earth element and Nd isotope evidence in iron formation from the 2.9 Ga Pongola Supergroup, South Africa. Geochim. Cosmochim. Acta 72, 378–394.
Alibo, D.S., Nozaki, Y., 1999. Rare earth elements in seawater: particle association, shale-normalization, and Ce oxidation. Geochim. Cosmochim. Acta 63, 363–372.
Aspler, L.B., Chiarenzelli, J.R., 1998. Two Neoarchean supercontinents? Evidence from the Paleoproterozoic. Sediment. Geol. 120, 75–104.
Basta, F.F., Maurice, A.E., Fontboté, L., Favarger, P.Y., 2011. Petrology and geochemistry of the banded iron formation (BIF) of Wadi Karim and Um Anab, Eastern Desert Egypt: implications for the origin of Neoproterozoic BIF. Precambrian Res. 187, 277–292.
Bau, M., 1991. Rare-earth element mobility during hydrothermal and metamorphic fluid–rock interaction and the significance of the oxidation state of europium. Chem. Geol. 93, 219–230.

Bau, M., Dulski, P., 1996. Distribution of yttrium and rare-earth elements in the Penge and Kuruman iron-formations, Transvaal Supergroup South Africa. Precambrian Res. 79, 37–55.
Bau, M., Dulski, P., 1999. Comparing yttrium and rare earths in hydrothermal fluids from the Mid-Atlantic Ridge: implications for Y and REE behaviour during near-vent mixing and for the Y/Ho ratio of Proterozoic seawater. Chem. Geol. 155, 77–90.
Bau, M., Möller, P., 1993. Rare earth element systematics of the chemically precipitated component in early precambrian iron formations and the evolution of the terrestrial atmosphere–hydrosphere–lithosphere system. Geochim. Cosmochim. Acta 57, 2239–2249.
Bau, M., Koschinsky, A., Dulski, P., Hein, J.R., 1996. Comparison of the partitioning behaviours of yttrium, rare earth elements, and titanium between hydrogenetic marine ferromanganese crusts and seawater. Geochim. Cosmochim. Acta 60, 1709–1725.
Bekker, A., Holland, H., Wang, P.L., Rumble, D., Stein, H., Hannah, J., Coetzee, L., Beukes, N., 2004. Dating the rise of atmospheric oxygen. Nature 427, 117–120.
Bekker, A., Slack, J.F., Planavsky, N., Krapež, B., Hofmann, A., Konhauser, K.O., Rouxel, O.J., 2010. Iron formation: the sedimentary product of a complex interplay among mantle, tectonic, oceanic, and biospheric processes. Econ. Geol. 105, 467–508.
Bleeker, W., 2003. The late Archean record: a puzzle in ca. 35 pieces. Lithos 71, 99–134.
Bolhar, R., Kamber, B.S., Moorbath, S., Fedo, C.M., Whitehouse, M.J., 2004. Characterisation of early Archean chemical sediments by trace element signatures. Earth Planet. Sci. Lett. 222, 43–60.
Bradley, D.C., 2011. Secular trends in the geologic record and the supercontinent cycle. Earth Sci. Rev. 108, 16–33.
Byrne, R.H., Kim, K.H., 1990. Rare earth element scavenging in seawater. Geochim. Cosmochim. Acta 54, 2645–2656.
Cairnssmith, A.G., 1978. Precambrain solution photochemistry, inverse segregation, and banded iron formations. Nature 276, 807–808.
Current progresses in indications of crustal composition and sedimentary environment and their evolutions with sedimentary trace elements. In: Chen, Y.J. (Ed.), Geol. Geochem., 3, pp. 1–125 (in Chinese).
Chen, Y.J., Fu, S.G., 1991. Variation of REE patterns in early Precambrian sediments: theoretical study and evidence from the southern margin of the northern China Craton. Chin. Sci. Bull. 36, 1100–1104.
Chen, Y.J., Zhao, Y.C., 1997. Geochemical characteristics and evolution of REE in the Early Precambrian sediments: evidences from the southern margin of the North China Craton. Episodes 20, 109–116.
Chen, F., Zhu, X.Q., 1984. Simulating experiment on the mechanism of formation of banded iron–silicon formations: weathering and leaching of basalts. Geochimica 13, 341–349 (in Chinese with English abstract).
Chen, G.Y., Sun, D.S., Sun, C.M., Li, M.H., Wang, X.F., Wang, Z.F., 1984. Genesis of Gongchangling iron deposit. J. Mineral. Petrol. 4, 1–266 (in Chinese).
Chen, J.F., Yang, Y.L., Li, P., Cheng, W.J., Zhou, T.X., Liu, Y.P., 1985. Sulfur isotope study on the genesis of high-grade iron deposit in Anshan–Benxi area, Liaoning Province. Geol. Prospect. 21, 32–37 (in Chinese).
Chen, Y.J., Ji, H.Z., Zhou, X.P., Fu, S.G., 1991. The challenge to the traditional geological theories from revelation of the catastrophe at 2300 Ma: new knowledge on several important geological subjects. Adv. Earth Sci. 6, 63–68 (in Chinese with English abstract).
Chen, Y.J., Fu, S.G., Hu, S.X., Zhang, Y.Y., 1992. The REE geochemical evolution and its significance of the Wuyang early Precambrian metamorphic terrain. Chin. J. Geochem. 11, 133–139.
Chen, Y.J., Ouyang, Z.Y., Yang, Q.J., Deng, J., 1994. A new understanding of the Archean–Proterozoic boundary. Geol. Rev. 40, 483–488 (in Chinese with English abstract).
Chen, Y.J., Yang, J.Q., Deng, J., Ji, H.Z., Fu, S.G., Zhou, X.P., Lin, Q., 1996. An important change in Earth's evolution: an environmental catastrophe at 2300 Ma and its implications. Geol. Geochem. 3, 106–128 (in Chinese).
Cheng, Y.Q., 1957. Problems on the high-grade ore in the Presinian (Precambrian) banded iron ore deposits of the Anshan type of Liaoning and Shandong Provinces. Acta Geol. Sin. 33, 153–180 (in Chinese with English abstract).
Chi, W.Z., 1993. Second mining area of Gongchangling iron deposit. Chinese Iron Ore Deposit. Metallurgical Industry Press, Beijing, pp. 279–284 (in Chinese).
Cloud, P., 1973. Paleoecological significance of banded iron formation. Econ. Geol. 68, 1135–1143.
Condie, K.C., Belousova, E., Griffin, W., Sircombe, K.N., 2009. Granitoid events in space and time: constraints from igneous and detrital zircon age spectra. Gondwana Res. 15, 228–242.
Craddock, P.R., Dauphas, N., 2011. Iron and carbon isotope evidence for microbial iron respiration throughout the Archean. Earth Planet. Sci. Lett. 303, 121–132.
Danielson, A., Möller, P., Dulski, P., 1992. The europium anomalies in banded iron formations and the thermal history of the oceanic crust. Chem. Geol. 97, 89–100.
Farquhar, J., Wing, B.A., 2003. Multiple sulfur isotopes and the evolution of the atmosphere. Earth Planet. Sci. Lett. 213, 1–13.
Frost, B.R., Tracy, R.J., 1991. PT paths from zoned garnets: some minimum criteria. Am. J. Sci. 291, 917–939.
Geng, Y., Liu, F., Yang, C., 2006. Magmatic event at the end of the Archean in eastern Hebei Province and its geological implication. Acta Geol. Sin. 80, 819–833.
Gonzalez, P.D., Sato, A.M., Llambias, E.J., Petronilho, L.A., 2009. Petrology and geochemistry of the banded iron formation in the Eastern Sierras Pampeanas of San Luis (Argentina): implications for the evolution of the Nogoli Metamorphic Complex. J. S. Am. Earth Sci. 28, 89–112.
Grant, M.L., Wilde, S.A., Wu, F.Y., Yang, J.H., 2009. The application of zircon cathodoluminescence imaging, Th–U–Pb chemistry and U–Pb ages in interpreting discrete magmatic and high-grade metamorphic events in the North China Craton at the Archean/Proterozoic boundary. Chem. Geol. 261, 155–171.
Gromet, L.P., Haskin, L.A., Korotev, R.L., Dymek, R.F., 1984. The "North American shale composite": its compilation, major and trace element characteristics. Geochim. Cosmochim. Acta 48, 2469–2482.
Gross, G.A., 1980. A classification of iron formations based on depositional environments. Can. Mineral. 18, 215–222.
Guan, G.Y., 1961. The significance of metamorphism in the genesis of high-grade iron ore. Acta Geol. Sin. 41, 65–76 (in Chinese with Russian abstract).
Holland, H.D., 2002. Volcanic gases, black smokers, and the great oxidation event. Geochim. Cosmochim. Acta 66, 3811–3826.
Holland, T., Blundy, J., 1994. Non-ideal interactions in calcic amphiboles and their bearing on amphibole–plagioclase thermometry. Contrib. Mineral. Petrol. 116, 433–447.
Huston, D.L., Logan, G.A., 2004. Barite BIFs and bugs: evidence for the evolution of the Earth's early hydrosphere. Earth Planet. Sci. Lett. 220, 41–55.
James, H.L., 1954. Sedimentary facies of iron-formation. Econ. Geol. 49, 235–293.
Jin, S.Q., 1991. Calcic amphibole compositional characteristics in different regional metamorphic facies. Chin. Sci. Bull. 36, 851–854 (in Chinese).
Kato, Y., Kawakami, T., Kano, T., Kunugiza, K., Swamy, N.S., 1996. Rare-earth element geochemistry of banded iron formations and associated amphibolite from the Sargur belts, south India. J. Southeast Asian Earth Sci. 14, 161–164.
Khan, R.M.K., Das Sharma, S., Patil, D.J., Naqvi, S.M., 1996. Trace, rare-earth element, and oxygen isotopic systematics for the genesis of banded iron-formations: evidence from the Kushtagi schist belt, Archaean Dharwar Craton India. Geochim. Cosmochim. Acta 60, 3285–3294.
Klein, C., 2005. Some Precambrian banded iron-formations (BIFs) from around the world: their age, geologic setting, mineralogy, metamorphism, geochemistry, and origin. Am. Mineral. 90, 1473–1499.
Klein, C., Beukes, N.J., 1989. Geochemistry and sedimentology of a facies transition from limestone to iron-formation deposition in the early Proterozoic Transvaal Supergroup, South Africa. Econ. Geol. 84, 1733–1774.
Kröner, A., Wilde, S.A., Li, J.H., Wang, K.Y., 2005. Age and evolution of a late Archean to Paleoproterozoic upper to lower crustal section in the Wutaishan/Hengshan/Fuping terrain of northern China. J. Asian Earth Sci. 24, 577–595.
Kusky, T.M., Li, J.H., Tucker, R.D., 2001. The Archean Dongwanzi ophiolite complex, North China craton: 2.505-billion-year-old oceanic crust and mantle. Science 292, 1142–1145.
Lascelles, D.F., 2007. Black smokers and density currents: an uniformitarian model for the genesis of banded iron-formations. Ore Geol. Rev. 32, 381–411.
Leake, B.E., Woolley, A.R., Arps, C.E.S., Birch, W.D., Gilbert, M.C., Grice, J.D., Hawthorne, F.C., Kato, A., Kisch, H.J., Krivovichev, V.G., Linthout, K., Laird, J., Mandarino, J., Maresch, W.V., Nickel, E.H., Rock, N.M.S., Schumacher, J.C., Smith, D.C., Stephenson, N.C.N., Ungaretti, L., Whittaker, E.J.W., Guo, Y.Z., 1997. Nomenclature of amphiboles: report of the subcommittee on amphiboles of the International Mineralogical Association, Commission on New Minerals and Mineral Names. Eur. J. Mineral. 9, 623–651.
Li, S.B., 1979. A contribution to the genesis of rich magnetite deposit of the Gongchangling type: in the light of graphite discovery in it. Geochimica 8, 170–177 (in Chinese with English abstract).
Li, S.G., 1982. Geochemical model for the genesis of the Gongchangling rich magnetite deposit in China. Geochimica 11, 113–121 (in Chinese with English abstract).
Li, B.L., Li, X.M., Cui, X.F., Wang, Z.L., 1977. Fluid inclusions thermometry of mineral from Gongchangling No. 2 mining area. J. Univ. Sci. Tech China 7, 96–103 (in Chinese).
Li, S.G., Zhi, C.X., Chen, J.F., Wang, J.X., Deng, Y.Y., 1983. Origin of graphites in early Precambrian banded iron formation in Anshan, China. Geochimica 12, 162–169 (in Chinese with English abstract).
Li, J.H., Hou, G.T., Huang, X.N., Zhang, Z.Q., Qian, X.L., 2001. The constraint for the supercontinental cycles: evidence from Precambrian geology of North China Block. Acta Petrol. Sin. 17, 177–186 (in Chinese with English abstract).
Li, Y.H., Hou, K.J., Wan, D.F., Zhang, Z.J., 2010. Formation mechanism of Precambrian banded iron formation and atmosphere and ocean during early stage of the Earth. Acta Geol. Sin. 84, 1359–1373 (in Chinese with English abstract).
Li, H.M., Liu, M.J., Li, L.X., Yang, X.Q., Chen, J., Yao, L.D., Hong, X.K., Yao, T., 2012. Geology and geochemistry of the marble in the Gongchangling iron ore deposit in Liaoning Province and their metallogenic significance. Acta Petrol. Sin. 28, 3497–3512 (in Chinese with English abstract).
Liu, J., Jin, S.Y., 2010. Genesis study of magnetite-rich ore in Gongchangling iron deposit, Liaoning. Geoscience 24, 80–88 (in Chinese with English abstract).
Liu, D.Y., Nutman, A.P., Compston, W., Wu, J.S., Shen, Q.H., 1992. Remnants of ≥3800 Ma crust in the Chinese part of the Sino-Korean craton. Geology 20, 339–342.
McLennan, S.M., 1989. Rare earth elements in sedimentary rocks: influence of provenance and sedimentary processes. In: Lipin, B.R., McKay, G.A. (Eds.), Geochemistry and mineralogy of rear earth elements. Rev. Mineral. Geochem, 21, pp. 169–200.
Mojzsis, S.J., Arrhenius, G., McKeegan, K.D., Harrison, T.M., Nutman, A.P., Friend, C.R.L., 1996. Evidence for life on Earth before 3,800 million years ago. Nature 384, 55–59.
Nozaki, Y., Zhang, J., Amakawa, H., 1997. The fractionation between Y and Ho in the marine environment. Earth Planet. Sci. Lett. 148, 329–340.
Posth, N.R., Hegler, F., Konhauser, K.O., Kappler, A., 2008. Alternating Si and Fe deposition caused by temperature fluctuations in Precambrian oceans. Nat. Geosci. 1, 703–708.
Powell, R., Holland, T., Worley, B., 1998. Calculating phase diagrams involving solid solutions via non-linear equations, with examples using THERMOCALC. J. Metamorph. Geol. 16, 577–588.
Qi, L., Gregoire, D.C., 2000. Determination of trace elements in twenty six Chinese geochemistry reference materials by inductively coupled plasma-mass spectrometry. Geostand. Newslett. 24, 51–63.
Rogers, J.J.W., Santosh, M., 2003. Supercontinents in Earth history. Gondwana Res. 6, 357–368.

Shen, Q.H., 1998. Geological characteristics and tectonic setting of the Early Precambrian BIFs in the North China Craton. In: Chen, Y.Q. (Ed.), The Early Precambrian Geological Study on the North China Craton Conference Proceeding. Geological Publishing House, Beijing, pp. 1–30 (in Chinese).
Shi, J.X., Li, B.C., 1980. Origin of rich magnetite ores in the Gongchangling area as evidenced by fluid inclusion studies from the Anshan–Benxi region, Northeast China. Geochimica 9, 43–53 (in Chinese with English abstract).
Slack, J.F., Cannon, W.F., 2009. Extraterrestrial demise of banded iron formations 1.85 billion years ago. Geology 37, 1011–1014.
Song, B., Nutman, A.P., Liu, D.Y., Wu, J.S., 1996. 3800 to 2500 Ma crustal evolution in the Anshan area of Liaoning Province, northeastern China. Precambrian Res. 78, 79–94.
Spear, F., 1991. On the interpretation of peak metamorphic temperatures in light of garnet diffusion during cooling. J. Metamorph. Geol. 9, 379–388.
Sun, S.S., McDonough, W.F., 1989. Chemical and isotopic systematics of oceanic basalts: implications for mantle composition and processes. In: Saunders, A.D., Norry, M.J. (Eds.), Magmatism in the Ocean Basins. Geological Society, London, Special Publications, 42, pp. 313–345.
Sun, X.H., Zhu, X.Q., Tang, H.S., Zhang, Q., Luo, T.Y., Han, T., 2014. Protolith reconstruction and geochemical study on the wall rocks of Anshan BIFs, Northeast China: implications for the provenance and tectonic setting. J. Geochem. Explor. 136, 65–75.
Tang, H.S., Chen, Y.J., 2013. Global glaciations and atmospheric change at ca. 2.3 Ga. Geosci. Front. 4, 583–596.
Tang, H.S., Chen, Y.J., Wu, G., Lai, Y., 2008. The C–O isotope composition of the Liaohe Group, northern Liaoning province and its geologic implications. Acta Petrol. Sin. 24, 129–138 (in Chinese with English abstract).
Tang, H.S., Chen, Y.J., Wu, G., Yang, T., 2009a. Rare earth element geochemistry of carbonates of Dashiqiao Formation, Liaohe Group, eastern Liaoning province: implications for Lomagundi Event. Acta Petrol. Sin. 25, 3075–3093 (in Chinese with English abstract).
Tang, H.S., Wu, G., Lai, Y., 2009b. The C–O geochemistry and genesis of the Dashiqiao magnesite deposit, Liaoning Province, NE China. Acta Petrol. Sin. 25, 455–467 (in Chinese with English abstract).
Tang, H.S., Chen, Y.J., Wu, G., Lai, Y., 2011. Paleoproterozoic positive δ^{13}Ccarb excursion in the northeastern Sino-Korean craton: evidence of the Lomagundi Event. Gondwana Res. 19, 471–481.
Tang, H.S., Chen, Y.J., Santosh, M., Zhong, H., Wu, G., Lai, Y., 2013a. C–O isotope geochemistry of the Dashiqiao magnesite belt, North China Craton: implications for the Great Oxidation Event and ore genesis. Geol. J. 48, 467–483.
Tang, H.S., Chen, Y.J., Santosh, M., Zhong, H., Yang, T., 2013b. REE geochemistry of carbonates from the Guanmenshan Formation, Liaohe Group NE Sino-Korean Craton: implications for seawater compositional change during the Great Oxidation Event. Precambrian Res. 227, 316–336.
Taylor, S.R., McLennan, S.M., 1985. The Continental Crust: Its Composition and Evolution. Blackwell, Oxford (312 pp.).
Taylor, S.R., McLennan, S.M., 1995. The geochemical evolution of the continental crust. Rev. Geophys. 33, 241–265.
Trendall, A.F., Blockley, J.G., 1970. The iron formations of the Precambrian Hamersley Group Western Australia with special reference to the crocidolite. Geological Survey of Western Australia Bulletin, Perth 365 p.
Walker, J.C.G., 1984. Suboxic diagenesis in banded iron formations. Nature 309, 340–342.
Wan, Y.S., 1994. Formation and evolution of the iron-bearing rock series of Gongchangling area Liaoning Province. Beijing Science and Technology Press, Beijing 108 p.
Wan, Y.S., Liu, D.Y., Wang, S.J., Yang, E.X., Wang, W., Dong, C.Y., Zhou, H.Y., Du, L.L., Yang, Y.H., Diwu, C.R., 2011. 2.7 Ga juvenile crust formation in the North China Craton (Taishan–Xintai area, western Shandong Province): further evidence of an understated event from U–Pb dating and Hf isotopic composition of zircon. Precambrian Res. 186, 169–180.
Wan, Y.S., Dong, C.Y., Liu, D.Y., Kröner, A., Yang, C.H., Wang, W., Du, L.L., Xie, H.Q., Ma, M.Z., 2012a. Zircon ages and geochemistry of late Neoarchean syenogranites in the North China Craton: a review. Precambrian Res. 222–223, 265–289.
Wan, Y.S., Dong, C.Y., Xie, H.Q., Wang, S.J., Song, M.C., Xu, Z.Y., Wang, S.Y., Zhou, H.Y., Ma, M.Z., Liu, D.Y., 2012b. Formation ages of early Precambrian BIFs in the North China Craton: SHRIMP zircon U–Pb dating. Acta Geol. Sin. 86, 1447–1478 (in Chinese with English abstract).
Wang, Z.G., Yu, X.Y., Zhao, Z.H., 1989. Rare Earth Elements Geochemistry. Science Press, Beijing (535 p (in Chinese)).
Wang, E.D., Xia, J.M., Zhao, C.F., Fu, J.F., Hou, B.G., 2012. Forming mechanism of high-grade magnetite bodies in Gongchangling. Liaoning. Acta Geol. Sin. 86, 1761–1772 (in Chinese with English abstract).
Wang, E.D., Xia, J.M., Zhao, C.F., Fu, J.F., Hou, B.G., 2013. Material source and sedimentary environment of Gongchangling iron deposit. Miner. Deposits 32, 380–396 (in Chinese with English abstract).
Wilde, S.A., Cawood, P.A., Wang, K., Nemchin, A.A., 2005. Granitoid evolution in the Late Archean Wutai Complex North China Craton. J. Asian Earth Sci. 24, 597–613.
Williams, H., Hoffman, P.F., Lewry, J.F., Monger, J.W.H., Rivers, T., 1991. Anatomy of North America: thematic geologic portrayals of the continent. Tectonophysics 187, 117–134.
Wonder, J.D., Spry, P.G., Windom, K.E., 1988. Geochemistry and origin of manganese-rich rocks related to iron-formation and sulfide deposits, western Georgia. Econ. Geol. 83, 1070–1081.
Xie, C.X., Li, H.M., Wang, R.J., Xiao, K.Y., 2009. Analysis of the quality and distribution of total identified iron resources in China and their supply capability. Acta Geosci. Sin. 30, 387–394 (in Chinese with English abstract).
Yang, J.H., Wu, F.Y., Wilde, S.A., Zhao, G.C., 2008. Petrogenesis and geodynamics of Late Archean magmatism in eastern Hebei, eastern North China Craton: geochronological, geochemical and Nd–Hf isotopic evidence. Precambrian Res. 167, 125–149.
Young, G.M., 2013. Precambrian supercontinents, glaciations, atmospheric oxygenation, metazoan evolution and an impact that may have changed the second half of Earth history. Geosci. Front. 4, 247–261.
Zhai, M.G., 2010. Tectonic evolution and metallogenesis of the North China Craton. Miner. Deposits 29, 24–36 (in Chinese with English abstract).
Zhai, M.G., 2011. Cratonization and the Ancient North China Continent: a summary and review. Sci. China Ser. D 54, 1110–1120.
Zhai, M.G., Santosh, M., 2011. The early Precambrian odyssey of the North China Craton: a synoptic overview. Gondwana Res. 20, 6–25.
Zhai, M.G., Santosh, M., 2013. Metallogeny of the North China Craton: link with secular changes in the evolving Earth. Gondwana Res. 24, 275–297.
Zhai, M.G., Windley, B.F., 1990. The Archean and early Proterozoic banded iron formations of North China: their characteristics, geotectonic relations, chemistry and implications for crustal growth. Precambrian Res. 48, 267–286.
Zhai, M.G., Windley, B.F., Sills, J.D., 1990a. Archean gneisses, amphibolites and banded iron-formations from the Anshan area of Liaoning Province, NE China: their geochemistry, metamorphism and petrogenesis. Precambrian Res. 46, 195–216.
Zhai, M.G., Sills, J.D., Windley, B.F., 1990b. Metamorphic mineral and metamorphism of the Anshan Group in Anshan–Benxi area Liaoning. Acta Petrol. Mineral. 9, 148–158 (in Chinese with English abstract).
Zhai, M.G., Bian, A.G., Zhao, T.P., 2000. The amalgamation of the supercontinent of North China Craton at the end of Neoarchean and its breakup during late Palaeoproterozoic and Mesoproterozoic. Sci. China Ser. D 43, 219–232.
Zhai, M.G., Guo, J.H., Liu, W.J., 2005. Neoarchean to Paleoproterozoic continental evolution and tectonic history of the North China Craton: a review. J. Asian Earth Sci. 24, 547–561.
Zhang, Z.M., Yang, Y., Zhang, J.X., 2000. The compositional zoning of garnet in eclogite from western segment of Altyn Tagh, northwestern China and its dynamic significance. Chin. Sci. Bull. 45, 79–83.
Zhang, X.J., Zhang, L.C., Xiang, P., Wan, B., Pirajno, F., 2011. Zircon U–Pb age, Hf isotopes and geochemistry of Shuichang Algoma-type banded iron-formation North China Craton: constraints on the ore-forming age and tectonic setting. Gondwana Res. 20, 137–148.
Zhang, L.C., Zhai, M.G., Wan, Y.S., Guo, J.H., Dai, Y.P., Wang, C.L., Liu, L., 2012a. Study of Precambrian BIF-iron deposits in North China Craton: progress and questions. Acta Petrol. Sin. 28, 3431–3445 (in Chinese with English abstract).
Zhang, L.C., Zhai, M.G., Zhang, X.J., Xiang, P., Dai, Y.P., Wang, C.L., Pirajno, F., 2012b. Formation age and tectonic setting of the Shirengou Neoarchean banded iron deposit in eastern Hebei Province: constraints from geochemistry and SIMS zircon U–Pb dating. Precambrian Res. 222–223, 325–338.
Zhao, B., Li, T.J., 1980. A preliminary study on the mechanism and physico-chemical conditions of the formation of the Gongchangling rich iron deposit. Geochimica 9, 333–344 (in Chinese with English abstract).
Zhao, G.C., 2009. Metamorphic evolution of major tectonic units in the basement of the North China Craton: key issues and discussion. Acta Petrol. Sin. 25, 1772–1992 (in Chinese with English abstract).
Zhao, G.C., Zhai, M.G., 2013. Lithotectonic elements of Precambrian basement in the North China Craton: review and tectonic implications. Gondwana Res. 23, 1207–1240.
Zhao, B., Wang, S.Y., Li, T.J., 1979. The origin of migmatite granite and its relationship with iron deposit: an experimental study. Geochimica 8, 211–221 (in Chinese with English abstract).
Zhao, G.C., Wilde, S.A., Cawood, P.A., Lu, L., 1998. Thermal evolution of Archean basement rocks from the eastern part of the North China Craton and its bearing on tectonic setting. Int. Geol. Rev. 40, 706–721.
Zhao, G.C., Sun, M., Wilde, S.A., 2003. Correlations between the eastern block of the North China craton and the south Indian block of the Indian Shield: an Archean to Palaeoproterozoic link. Precambrian Res. 122, 201–233.
Zhao, G.C., Sun, M., Wilde, S.A., Li, S.Z., 2005. Late Archean to Paleoproterozoic evolution of the North China Craton: key issues revisited. Precambrian Res. 136, 177–202.
Zhao, Z.H., 2010. Banded iron formation and related great oxidation event. Earth Sci. Front. 17, 1–12 (in Chinese with English abstract).
Zheng, Y.F., Xiao, W.J., Zhao, G.C., 2013. Introduction to tectonics of China. Gondwana Res. 23, 1189–1206.
Zhou, S.T., 1987. The petrochemical study of the Archean banded iron deposit in Anshan–Benxi district, Liaoning Province. Bull. Chin. Acad. Geol. Sci. 16, 139–153 (in Chinese with English abstract).
Zhou, S.T., 1994. Geology of Banded Iron Formations in Anshan–Benxi Area. Geological Publishing House, Beijing 278 p. (in Chinese).
Zhou, S.T., 1997. The research progress and forecasting of Chinese Archean banded iron formation. Geol. Prospect. 33, 1–7 (in Chinese with English abstract).